Nano Research

ISSN 1998-0124 CN 11-5974/O4
https://doi.org/10.1007/s12274-021-3405-0

Perspective Review

Graphene: A promising candidate for charge regulation in high-performance lithium-ion batteries

Danping Sun[1,2,§] Zhi Tan[2,§], Xuzheng Tian[2], Fei Ke[2], Yale Wu[2], and Jin Zhang[1,2] (✉)

[1] *College of Chemistry and Molecular Engineering, Beijing Science and Engineering Center for Nanocarbons, Beijing National Laboratory for Molecular Sciences, Peking University, Beijing 100871, China*
[2] *Beijing Graphene Institute (BGI), Beijing 100095, China*
[§] *Danping Sun and Zhi Tan contributed equally to this work.*

Received: 25 January 2021 / **Revised:** 13 February 2021 / **Accepted:** 15 February 2021

ABSTRACT

The development of rechargeable lithium-ion batteries (LIBs) is being driven by the ever-increasing demand for high energy density and excellent rate performance. Charge transfer kinetics and polarization theory, considered as basic principles for charge regulation in the LIBs, indicate that the rapid transfer of both electrons and ions is vital to the electrochemical reaction process. Graphene, a promising candidate for charge regulation in high-performance LIBs, has received extensive investigations due to its excellent carrier mobility, large specific surface area and structure tunability, etc. Recent progresses on the structural design and interfacial modification of graphene to regulate the charge transport in LIBs have been summarized. Besides, the structure-performance relationships between the structure of the graphene and its dedicated applications for LIBs have also been clarified in detail. Taking graphene as a typical example to explore the mechanism of charge regulation will outline ways to further understand and improve carbon-based nanomaterials towards the next generation of electrochemical energy storage devices.

KEYWORDS

graphene, charge transport, lithium-ion battery, electron and ion transfer

1 Introduction

The rapid development of electric devices has triggered the dramatically increasing demands for high energy density and excellent rate capability for lithium-ion batteries (LIBs) [1]. Considering that the performance of LIBs is mainly based on the electrochemical reaction in the electrode, designing advanced electrode materials as well as electrodes with optimized compositions and structures have become two crucial strategies to break through the energy density and fast charge limitation for commercial LIBs [2, 3].

Carbon-based nanocomposites have been regarded as the versatile platform for building superior LIBs with a higher energy density and rate capability due to their intriguing properties [4–8]. In particular, graphene, a typical two-dimensional (2D) carbon material consisting of one layer of honeycomb structured sp^2 carbon atoms, has received extensive investigations and wide application potentials in LIBs owing to extremely high carrier mobility, excellent electrical conductivity and high theoretical specific surface area [9, 10]. Although graphene can also be used as an active lithium storage material [11], in most cases, it is more like a regulator serving to manipulate the lithium storage behavior of a specific active material. Therefore, comprehensive understanding of the regulation principles of graphene would make for the realization of its killer applications in high-performance LIBs in the future.

It is well known that graphene plays an important role in regulating the charge transport including electron and ion transfer at the electrode interface of LIBs. Nevertheless, when adopting graphene as a regulator into the battery system to promote the battery performance, there still exist a lot of issues which hinder the full demonstration of the intrinsic conductivity of graphene. To realize the optimal use of graphene in LIBs, great efforts are needed for the rational design and modification of the structure and chemistry of graphene materials. The introduction of defects including intrinsic and extrinsic defects makes it possible to tailor the local properties of graphene for the purpose of simultaneous regulation of electron and ion transfer, as shown in Fig. 1. In addition, when developing graphene to boost the electrochemical property of the battery

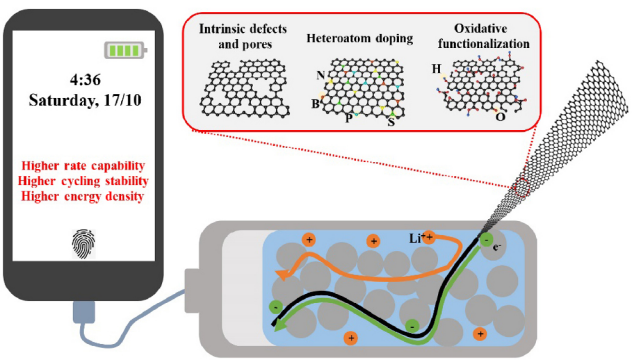

Figure 1 Charge regulation roles of modified graphene via defect engineering in LIBs.

Address correspondence to jinzhang@pku.edu.cn

system, the size matching between graphene and active particles needs to be taken into consideration due to the mutual effect of electron and ion transfer. Constructing graphene-based macrostructures, which consist of graphene sheets assembled according to a certain structure and orientation, can not only maintain excellent physicochemical properties of graphene, but also possess controllable micro-nano structures to widen the application range of graphene in LIBs.

At present, the regulation principles of graphene for the charge transport including the electron and ion transfer from the perspective of design and modification from the atomic level to macro level, have not been systematically explained and summarized. Herein, we begin with a brief introduction to the working principle of LIBs, focusing on the kinetic process in the electrode and related critical concepts including charge transfer, polarization and charge transport. Then we systematically discuss the design and modification strategies of graphene to regulate and facilitate the charge transport at the electrode interface from three aspects: 1) size modulation; 2) introduction of intrinsic or extrinsic defects in graphene; 3) design and construction of graphene-based macroscopic architectures. The relevant regulation principle has also been clarified in detail. Finally, various applications of graphene in LIBs, such as graphene-based composites, current collectors, and conductive agents, which further demonstrate the regulation role of graphene in battery performance, together with challenges of graphene-based materials have also been summarized. This review is specifically aimed at providing new perspectives on the rational structural design and modification of graphene for its optimal use in LIBs.

2 Principles and critical factors in electrode process of LIBs

2.1 Principles

LIBs consisting of an anode, a cathode, and a membrane which all immersed in the electrolyte [12], depend on the Li^+ to travel back and forth between the two electrodes for operation. To get further understanding about the working principle of LIBs during charge/discharge process, herein, the typical $LiFePO_4$/graphite battery is taken as an example, and the related electrode reactions are listed as Eqs. (1) and (2) [13]

$$x\mathrm{Li}^+ + \mathrm{Li}_{(1-x)}\mathrm{FePO}_4 + xe^- \rightleftharpoons \mathrm{LiFePO}_4 \quad (1)$$

$$\mathrm{Li}_x C_6 \rightleftharpoons x\mathrm{Li}^+ + C_6 + xe^- \quad (2)$$

When discharging (as illustrated in Fig. 2), electrons liberated from the graphite anode flow to the current collector via the external circuit, and then arrive at the interface of the $LiFePO_4$ (LFP) cathode through conductive agents, to provide the necessary electrons for the insertion half-reaction. During the electron liberation, the graphite is oxidized along with the de-intercalation of Li^+. The de-intercalated Li^+ subsequently diffuses across the bulk of electrolyte, via conductive agents, and reaches the interface of $LiFePO_4$ cathode to diffuse and intercalate into the bulk of $LiFePO_4$ materials. While in the charge process, a voltage is applied to drive the half reactions in the backward direction, where Li^+ derived from the $LiFePO_4$ cathode diffuses across the electrolyte, and finally inserts into the graphite anode [14].

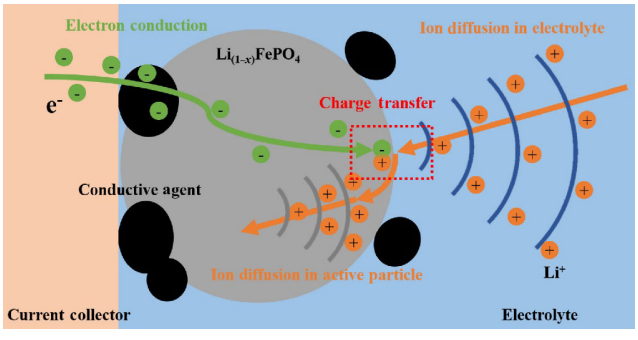

Figure 2 Schematic illustration of the kinetic process in the $LiFePO_4$ electrode.

As described above, the kinetic process in the $LiFePO_4$ electrode involves (1) the diffusion of electrons and Li^+ through the corresponding electron- and ion-conducting phases, (2) the diffusion of Li^+ through the electrode/electrolyte interface, (3) charge transfer at the electrode interface, and (4) the diffusion of Li^+ in the bulk of the cathode material. In particular, the charge transfer process (i.e., the electrochemical reaction occurring at the electrode interface), as highlighted in the red box in Fig. 2, plays an essential role in determining the performance of LIBs. To make a further clarification, the electrochemical reaction equation and the polarization theory are introduced, and for convenience, the reaction equation is simplified as Eq. (3) [15]

$$O + ne^- \rightleftharpoons R \quad (3)$$

Since the current is proportional to the reaction rate, the reaction rate could be expressed by the current and thus a dynamic formula can be obtained as Eq. (4) [15]

$$i = nFA(v_f - v_b) = nFA[k_f C_O(0,t)C_e(0,t)^n - k_b C_R(0,t)] \quad (4)$$

Where i denotes net current value, F is Faraday constant, A refers to the reaction area, k_f and k_b are forward and backward reaction rate constants, respectively. C_O, C_e, C_R are the instant concentrations of oxide O, electrons and reductant R near reaction interfaces. Of note, k_f, k_b, C_O, C_e, and C_R are the key variables that affect the reaction rate. For the electrode reactions, C_O, C_e, and C_R, the dynamic values over time, are influenced by the rate of charge transport and charge transfer itself, while rate constants k_f and k_b are often affected by applied potentials. According to Butler-Volmer theory [16], Eq. (4) could be converted to Eq. (5)

$$i = FAk^0[C_O(0,t)C_e(0,t)^n e^{-\alpha f(E-E^0)} - C_R(0,t)e^{(1-\alpha)f(E-E^0)}] \quad (5)$$

Where k^0 means standard rate constant, α denotes the transfer coefficient, E^0 and E refer to the operating voltage and standard cell voltage, respectively, $(E–E^0)$ denotes the applied potential. In fact, the operating voltage E is always lower than the standard cell voltage E^0 due to the polarization phenomenon, which could be stated mathematically as Eq. (6) [17]

$$E = E_0 - [(\eta_{ct})_a + (\eta_{ct})_c] - [(\eta_c)_a + (\eta_c)_c] - iR_i \quad (6)$$

Where $(\eta_{ct})_a$ and $(\eta_{ct})_c$ represent electrochemical active polarization at the anode and cathode, respectively, while $(\eta_c)_a$ and $(\eta_c)_c$ denote concentration polarization at the anode and cathode, respectively, and iR_i represents ohmic polarization. The electrochemical activation η_{ct} and concentration polarizations η_c are related to the kinetics of charge transfer and mass transfer [18–20], respectively, while the ohmic polarization iR_i is influenced by the intrinsic conductivities of various components. Such polarizations would slow the whole intercalation and de-intercalation kinetics of Li^+ and degrade the battery performance including capacity, rate performance, and cycling stability. Strategies to alleviate the polarization effect can be developed according to the above three polarization types: (1) the electrochemical activation polarization η_{ct}, (2) the concentration

polarization η_c, (3) the internal resistance R_i. The three polarizations share a common affecting factor, namely the charge transport (i.e., ionic and electronic transfer). Therefore, achieving fast charge transport might be a feasible approach to reducing the polarization effect and thus improving the battery performance.

2.2 Critical factors for achieving fast charge transport in LIBs

As discussed above, the fast charge transport in LIBs could promote the charge transfer reaction and mitigate the polarization effect at the electrode interface, thus leading to an improved battery performance. In order to provide a systematic understanding of charge transport to guide the relevant regulation strategies for high-performance LIBs, in this section, we will summarize the critical factors with respect to electrical and ionic transfer in the primary components in LIBs including cathodes, anodes, electrolytes and current collectors.

2.2.1 *Electronic conduction*

Electronic conduction is an important factor that affects the efficiency of charge transport. Internal electronic resistance in electrodes is determined by the electron transfer of material and the interfaces between various components. The electronic conduction can be divided into two parts, that is, the intrinsic conductivity of components and contact resistance between components [21].

Intrinsic conductivity of components

The intrinsic conductivities of different materials are determined by their own band structure [22–24]. For example, conductors have partially filled valence bands (metal) or small overlap between valence and conduction bands (semimetal), while insulators and semiconductors have fully filled valence bands and empty conduction bands with larger band gaps between the two bands. The electrical conductivities and band gaps of commonly used materials for LIBs are listed in Table 1.

Noted that most of the active materials (LFP, Si, LCO, etc.) are semiconductors with poor conductivity. Therefore, it is essential to incorporate conductive agents, such as carbon black, graphene, and carbon nanotubes, into the system to improve the overall conductivity of electrodes.

Table 1 Electrical conductivities and band gaps of various materials [25–31]

Material	Component	Band gap (eV)	Electrical conductivity ($S \cdot cm^{-1}$)	Ref.
Copper foil	Current collector	0	5.8×10^5	[25]
Aluminum foil	Current collector	0	3.4×10^5	[25]
Graphite	Anode	0	$(2–1)\times10^3$	[26]
Si	Anode	1.1–1.3	$<10^{-5}$	[27]
$LiCoO_2$	Cathode	0.5–2.7	$\sim10^{-4}$	[28]
$LiMn_2O_4$	Cathode	0.28–2.2	$\sim10^{-6}$	[29]
$LiFePO_4$	Cathode	0.3–1	$\sim10^{-9}$	[30]
S	Cathode	Insulator	5×10^{-30}	[31]

Contact resistance between components

Contact resistance generally refers to the impedance phenomenon caused by the poor contact between two components [32]. When two conductors are in contact with each other under a certain force, they seem to connect closely from a macroscopic perspective. However, due to the surface roughness and unevenness, contact between the two materials only distributed on a few discrete points in a microscopic view. In fact, the actual contact area at the interface usually accounts for less than 2% of apparent contact area [33]. When a current is generated by the applied potential, current will gather at the interface and pass through the discrete microcontact points. This process reduces the volume of conductor used for conduction, resulting in electrical contact resistance. Contact resistance widely exists in batteries, like contact between active material and current collector and contact between active particles. To alleviate the negative effect of contact resistance on the performance of LIBs, introduction of conductive agents like graphene and CNT can be useful as they possess large specific surface area, good flexibility, and excellent conductivity to enhance the contact area and to reduce the contact resistance [34].

2.2.2 *Ionic conduction*

Ionic conduction refers to ion directional diffusion in a specific electric field. In regards to the lithium-ion batteries, the movement of Li^+ can be divided into two categories: conduction in electrolytes and diffusion in the bulk of active materials [21].

Li-ion conduction in the electrolytes

There are three mechanisms for the conduction of Li^+ in the electrolytes: diffusion, electro-migration and convection. When there is reactions taking place, there will be a concentration gradient of a reactant in the solution. Diffusion is driven by the concentration gradients and its rate is determined by Fick's first law [35, 36]. The electromigration is the phenomenon that various ions in solution move in a certain direction under the electric field. The convection occurs when electrode reaction causes local concentration, changes in temperature as well as density differences in solution [15].

During the charging/discharging process, the three mechanisms mentioned above exist simultaneously. In areas far away from electrode surfaces, convection mechanism plays a major role. However, when approaching the surface of the electrode, the rate of convection is rather smaller than that of diffusion and electromigration and thus the latter become the vital factors. Also, when diving further into gaps of active components, Li^+ can be easily hindered by conductive components, like graphene and carbon nanotubes, which makes it difficult to transfer in the form of convection [15]. Therefore, rational design and modification scheme of graphene could be essential.

Li-ion diffusion in active particles

In fact, Li^+ diffusing in bulks, like that in electrolytes, belongs to diffusion mechanism in condensed matter field, which follows Fick's law as well. Noted that the mobility of Li^+ in active materials can be affected by crystal structures of active materials. For example, $LiFePO_4$ materials have one-dimensional (1D) transmission channels for Li^+, $LiCoO_2$ and graphite possess two-dimensional (2D) layered structures, and $LiMn_2O_4$ materials have three-dimensional (3D) tunnel arrays. The difference in transmission channel naturally affects the diffusion of Li^+, which endows the 2D layered $LiCoO_2$ with the highest ionic conductivity (10^{-10}–10^{-8} $cm^2 \cdot S^{-1}$) and $LiFePO_4$ with the lowest ionic conductivity (10^{-14}–10^{-15} $cm^2 \cdot S^{-1}$) [21, 30, 31, 37].

3 Regulating charge transport in LIBs through design and modification of graphene

To meet the growing demands for high energy density and fast charge capability for LIBs, one key is to accelerate the

electrochemical reaction of LIBs by promoting the charge transport, which depends critically on the rate of electron and ion transfer in the electrode interface, as mentioned in the previous chapter. Graphene, a typical 2D carbon material, by virtue of intrinsically superior electrical conductivity, high surface area, and structural flexibility, has been intensely studied for improving the performance of LIBs [38]. It is recognized that graphene plays an important role in regulating the electrochemical process at the reaction interface of LIBs. For instance, graphene can accelerate the electronic transmission at the interface among the poorly conductive active materials. In addition, it also reduces the contact resistance by guaranteeing good contact between the active materials and current collectors as well as contact between the active materials and the electrolyte, effectively decreasing polarization. Nevertheless, when incorporating graphene to boost the battery performance, the properties of graphene together with the practical restrictions of the batteries need to be considered simultaneously. Only focusing on the intrinsic properties of graphene does not conduce to its practical application. This could be explained by the fact that the graphene naturally tends to agglomerate and its six-ring planar structure would block the transport of Li^+ in the cases like $LiFePO_4$ [39], which will result in the inferior rate capability. Therefore, judicious choice of design and modification scheme of graphene for specific application system could be vital. In the following sub-sections, we will discuss the design and modification strategies of graphene (shown in Fig. 3) to regulate and facilitate the charge transport at the electrode interface in LIBs. The relevant regulation principle will also be clarified in detail.

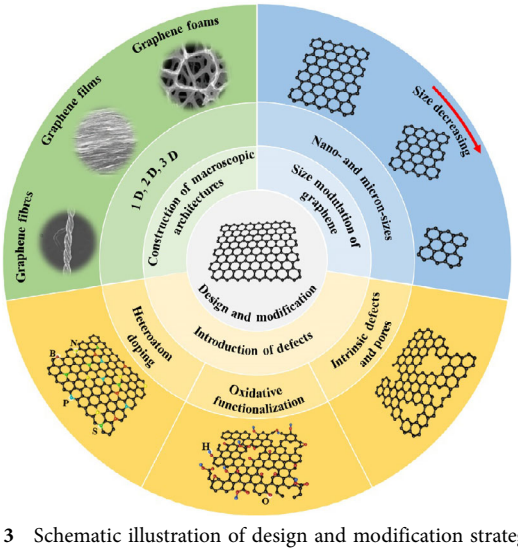

Figure 3 Schematic illustration of design and modification strategies of graphene.

3.1 Size modulation of graphene

From the perspective of the percolation theory [40], graphene with a larger size when used as conductive agent is easier to construct long-range conducting networks (as shown by the green arrows in Fig. 4(a) with less amount. However, graphene inherently tends to agglomerate owing to the strong π-π interaction between graphene layers [41], which hinders the full demonstration of its intrinsic conductivity and impairs the usage efficiency. In contrast, the small-sized graphene as conductive agent shows better dispersity and could provide more electric contact between graphene and active particles (Fig. 4(b)), though its electric conductivity is inferior than the one with large size. Therefore, in view of the two-sided nature of graphene with different sizes, a well-designed ratio of graphene

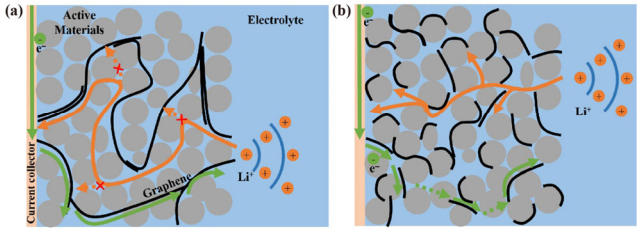

Figure 4 Effect of (a) graphene with large size and (b) graphene with small size on the transport of electrons and lithium ions in LIBs.

in two different sizes might be better for its real application as conductive agents. For example, Qi Li et al. prepared flexible paper with different sizes of graphene flakes [42]. They found that the flexible paper fabricated with a combination of large- and small-sized graphene showed dramatically improved electrical and thermal conductivities compared with the one prepared with single sized graphene. And they owed this result to the synergistic effect from the combination of large- and small-sized graphene, wherein, large sized graphene flakes play the role of a backbone structure, whereas small sized graphene flakes fill the voids in the paper.

In addition, it is worthwhile to mention that the planar structure of graphene could exert a steric hindrance effect for Li^+ diffusion (as indicated by the orange arrows in Fig. 4(a). For instance, Jianfei Wu et al. reported that the use of graphene in the $LiFePO_4$ would hinder the diffusion of Li^+ due to the prolonged transport paths [39]. Nevertheless, in another work, Quanhong Yang's group. demonstrated that no obvious blocking effect was found in the micro-sized $LiCoO_2$ even at high rate discharge, which was in contrary to the case of $LiFePO_4$ [43]. This phenomenon could be explained by the fact that the size ratio of graphene to active particles will influence the tortuosity of transport path, thus affecting the diffusion of Li^+. Given that the particle size of $LiCoO_2$ is one magnitude larger than $LiFePO_4$, the size ratio of graphene to the $LiFePO_4$ is quite larger than that of $LiCoO_2$, which causes prolonged transport path for Li^+ in $LiFePO_4$ electrode. Therefore, it is essential to select proper size of graphene according to the specific electrode system, and comprehensively consider the balance of electron and ion transfer when developing graphene for the use of regulating charge transport process in LIBs.

3.2 Introduction of defects in graphene

Perfect-structured graphene has shown an extremely high carrier mobility (200,000 $cm^2 \cdot V^{-1} \cdot s^{-1}$), excellent electrical conductivity (10^6 $S \cdot cm^{-1}$) and high theoretical surface area (2,630 $m^2 \cdot g^{-1}$), which makes it a promising candidate for various applications, such as energy storage materials and nanoelectronics [44–48]. Defects including intrinsic (e.g., vacancies, deformations, etc.) and extrinsic defects (e.g., O and H-containing groups, heteroatom like N, S, P, and B), which are inevitable to be introduced into the material during growth or treatment process, may deteriorate the actual performance of graphene in different applications. However, deviations from perfection, in some cases, can be favorable, as they make it possible to tailor the local properties of graphene for dedicated applications. For the purpose of promoting the charge transport process in LIBs, herein, we focus on three typical modification methods (Fig. 5) of graphene: engineering of intrinsic defects and pore structure, introduction of oxygen functional groups, and heteroatoms doping, which are classified according to the defect types as mentioned above. Thus, in the following sub-sections, we will discuss these modification schemes for graphene and elaborate their influences on the charge transport process in LIBs.

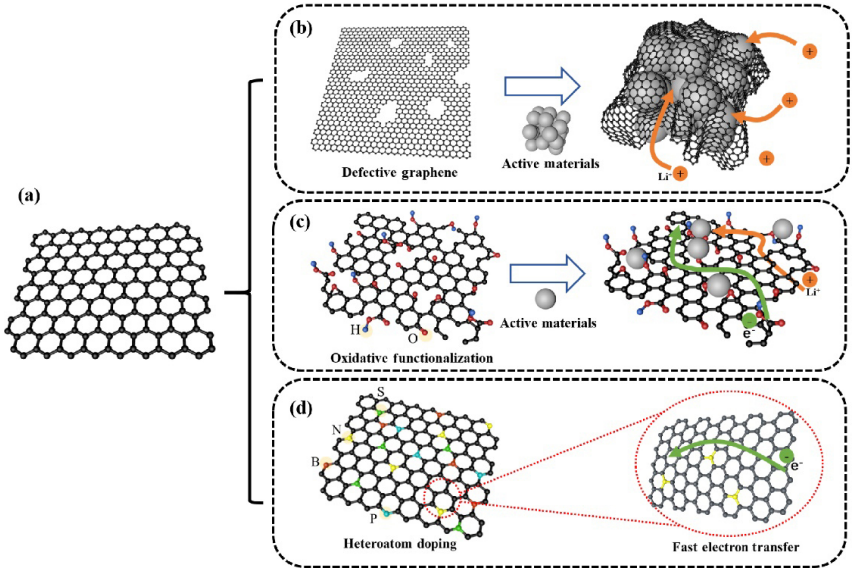

Figure 5 Pristine graphene and three typical modification strategies of graphene via the introduction of defects for use in promoting the charge transport in LIBs. (a) Schematic structure of a perfect-structured graphene matrix. (b) Introduction of defects and pores in graphene lattices to accelerate the penetration of electrolytes and the diffusion of Li^+. (c) Oxidative functionalization of graphene to generate anchor sites for the intimate contact between active materials and graphene oxide (or reduced graphene oxide) for efficient electron and ion transfer. (d) Doping with heteroatoms (N, S, B, P) in graphene lattices to tune the local electronic structure of graphene for fast electron transfer.

3.2.1 *Engineering of intrinsic defects and pore structure*

Intrinsic defects include vacancies [49, 50], edges [51], and deformations [52], which could be deliberately introduced into graphene by irradiation or chemical treatment [53–58]. Engineering of intrinsic defects in graphene could be utilized to regulate its local electronic structure, thus leading to an enhanced lithium storage performance [59, 60]. For instance, Vivek B. Shenoy et al. confirmed that the presence of defects in graphene could enhance Li adsorption due to the increased charge transfer between adatom and defective graphene through density functional theory (DFT) calculation [49]. More importantly, since defect-free graphene cannot allow the diffusion of Li^+ through its basal plane, engineering of defects with pore structure like vacancy defects could ensure high electrolyte accessibility and provides fast diffusion channels for Li^+ for an enhanced rate capability (shown in Fig. 5(b)) [61, 62].

The vacancy defects which are formed by the removal of carbon atoms could be readily introduced into the basal plane of graphene by ion or electron irradiation and chemical etching to facilitate the diffusion of Li^+ throughout the whole electrode. For example, Alex W. Robertson et al. developed an electron beam irradiation strategy to spatially control the vacancy defect formation in graphene [56]. Bin Ren et al. employed Ar^+ irradiation method to precisely introduce vacancy defects in graphene to quantitatively investigate the correlation between defect density and heterogeneous electron transfer (HET) rate [57]. An optimal HET rate constant was achieved at a defect density of $(7.39 \pm 0.58)\times10^{12}$ cm^{-2} by balancing the defect induced increase of DOS and decrease of conductivity of single layer graphene. In addition, Wei Huang et al. reported a facile and mild strategy to fabricate defect-enriched graphene mesh (GM) with in-plane pore sizes of 60–200 nm by Fe_2O_3 nanoparticles-assisted etching process [58]. They found that only the GMs electrodes with defect-induced pores can exhibit better Li storage performance in contrast to graphene aerogels, which revealed that both defect sites and porous structure are vital for the Li storage properties. Nevertheless, a high porosity and high conductivity often display a tradeoff relationship owing to the fact that excessive defect pore sizes and densities in graphene would otherwise damage the integrity of graphene sheet and give rise to poor electron transport resulted from the scattering effect [63–65]. Therefore, in order to gain an optimal balance between electrical conductivity and ionic transport, it is desirable to rationally control the pore sizes and densities of defects in graphene to finely tune the electrochemical properties of graphene for optimal use in LIBs.

3.2.2 *Introduction of oxygen functional groups*

Introduction of oxygen functional groups (such as epoxy, hydroxyl, carboxyl, and carbonyl groups) onto the basal plane and edge of graphene can be exploited to overcome the structural disadvantages of graphene such as low dispersibility and poor wettability between graphene and the electrolyte, thus leading to more efficient charge transport process in LIBs [66, 67]. The oxygen functional groups on the graphene surface guarantee the stable suspension of graphene on a variety of solvents and proffer sheet repulsion to prevent aggregation between layers. More importantly, the oxygen functional groups also function as an immobilizer in keeping good electrical contact between the active materials and the graphene matrix via covalent (e.g., –COO–) or non-covalent interactions (e.g., electrostatic and inductive interactions) to realize efficient electron transfer (Fig. 5(c)) for enhanced rate capability and cycling stability [68, 69]. For example, Yun Jung Lee et al. employed the negatively charged graphene oxide (GO) as starting templates via electrostatic interactions and subsequent *in-situ* polymerization reaction to obtain nanostructured $LiFePO_4$-reduced graphene oxide (rGO) hybrids (Figs. 6(a)–6(c)). The resulting hybrid cathodes showed superior rate capability and cyclability, in which the fast electron transport was enabled by the well-dispersed conducting networks of rGO and intimate contact between $LiFePO_4$ and conducting networks of rGO [70]. Xiangfeng Liu et al. proposed a subtle syn-graphenization strategy to fabricate $ZnFe_2O_4$-rGO hybrids (Figs. 6(d)–6(f)), where the highly conductive rGO allowed more electrons and Li^+ to diffuse into the electrode materials and the tight binding between $ZnFe_2O_4$ and rGO reduced the aggregation of $ZnFe_2O_4$ particles and lowered the contact resistance during the charge/discharge process, contributing to the excellent

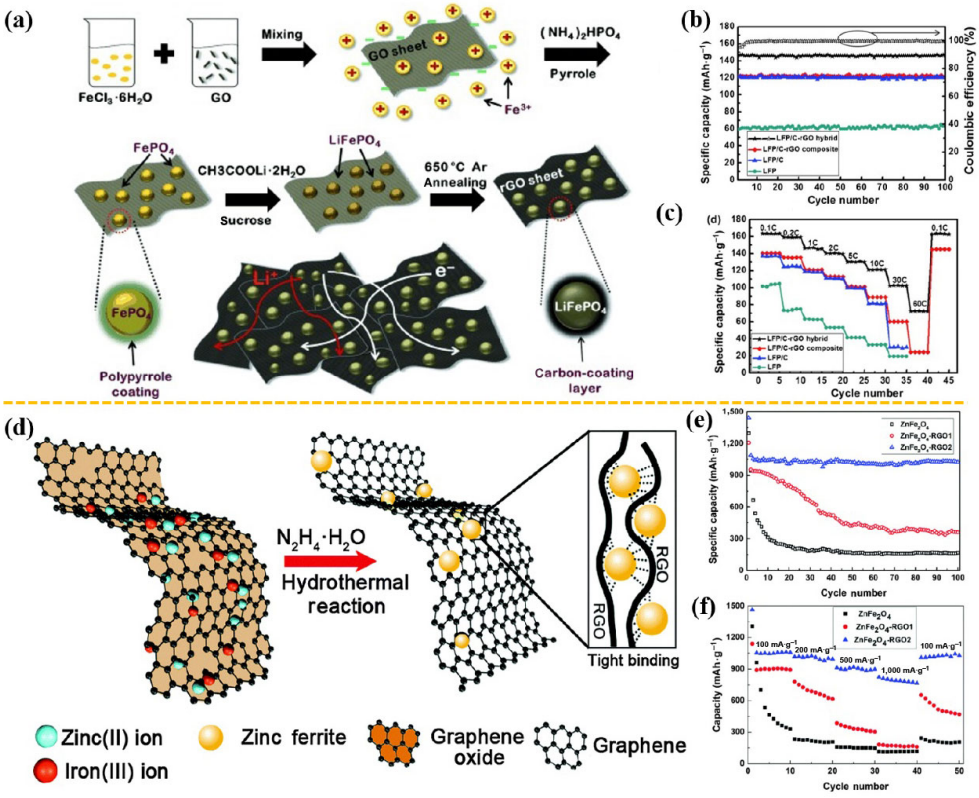

Figure 6 (a) Schematic illustration of the preparation of the LFP/C-rGO hybrid. (b) Capacity retention and coulombic efficiency and (c) rate capability comparison between LFP, LFP/C, LFP/C-rGO composite and LFP/C-rGO hybrid. Reproduced with permission from Ref. [70], © Wiley-VCH Verlag GmbH & Co. KGaA, Weinheim 2015. (d) Schematic representation of the preparation of $ZnFe_2O_4$-RGO hybrid via syn-graphenization strategy. (e) Cycling stability and (f) rate capacity of bulk $ZnFe_2O_4$, $ZnFe_2O_4$-RGO1 and $ZnFe_2O_4$-RGO. Reproduced with permission from Ref. [71], © The Royal Society of Chemistry 2016.

cyclability and rate capability [71].

However, the electronic conductivity of graphene mainly stems from the long-range π-conjugated structures in the carbon network, and oxidative functionalization which is inevitably along with the formation of defects will disrupt the π-conjugated electronic structure and affect the electrical transport, degrading the electrical conductivity of graphene [72]. In consequence, as-formed GO sheets are generally insulating [73]. Therefore, the poorly conductive GO, in practical application, is usually reduced to remove partial functional groups in order to yield highly conductive rGO for fast charge transport. Nevertheless, the conventional thermal annealing [74], or chemical reduction methods, for instance, the widely applied hydrazine [75], inevitably leads to the resulting rGO incorporating both lattice defects and residual oxidezed groups. The lattice defects originating from the leaving or substitution of oxygen functional groups and residual oxidized groups that are difficult to remove make it difficult to obtain highly conductive rGO. As a consequence, various approaches have been developed to recover the long-range conjugated structure in graphene lattice. Kwang-Bum Kim et al. proposed an efficient and scalable method involving microwave irradiation and heat treatment under NH_3 gas to successfully restore the π-conjugated structure of GO to obtain the nitrogen-doped rGO with high electrical conductivity (1,532 $S \cdot m^{-1}$), and low oxygen content (1.5 wt.%) [76]. In another work, Lopez et al. developed a CVD strategy to repair GO using ethylene as a carbon source, and the reduced GO exhibited a more than 50-fold increase in electrical conductivity compared with the GO reduced by conventional methods [77]. Zhongfan Liu et al. reported a real-time repair strategy to heal the newborn vacancies with carbon radicals produced by the thermal decomposition of precursors and the sheet conductivity of the monolayer graphene was raised more than six-fold to 350–410 $S \cdot cm^{-1}$ [78].

3.2.3 *Doping with heteroatoms (N, S, B, P)*

Extensive investigations reported that heteroatom doping with N, B, S, or P (Fig. 5(d)) is an effective strategy to tailor the electronic property of graphene by manipulating its local electronic structure, which could be instrumental to improve the electronic conductivity and wettability of graphene, thereby enhancing the transport of electrons and ions [79–81]. Huiming Cheng's group demonstrated a graphene-based anode material (Fig. 7) with an extremely high rate and a large capacity (> 1,040 $mAh \cdot g^{-1}$ at 50 $mA \cdot g^{-1}$) via heteroatom (N, B) doping strategy [81]. They confirmed that N or B doping could increase the electrical conductivity by the electrochemical impedance spectroscopy (EIS) test, wherein the N or B-doped graphene electrodes showed much lower electrolyte resistances and charge transfer resistances than those of un-doped graphene. Moreover, they also evaluated the wettability of the pristine and doped graphene by the contact angle test. The result showed that N or B-doped graphene exhibited increased electrode/electrolyte wettability than that of the pristine graphene, which facilitated ion diffusion at the interface between the electrode and electrolyte and the interior of bulk electrode. Following their research, Xi Wang et al. reported an atomistic insight of the N-doped graphene to elucidate its ultrafast lithium storage property [82]. They combined *in situ* high-resolution TEM together with theoretical calculations to prove that the ultrafast energy storage of N-doped graphene was due to the enhanced electrical conductivity and the improved surface capacitive effects resulted from enlarged edge {0002} spacings and surface hole defects after N-doping. Moreover, they also investigated the

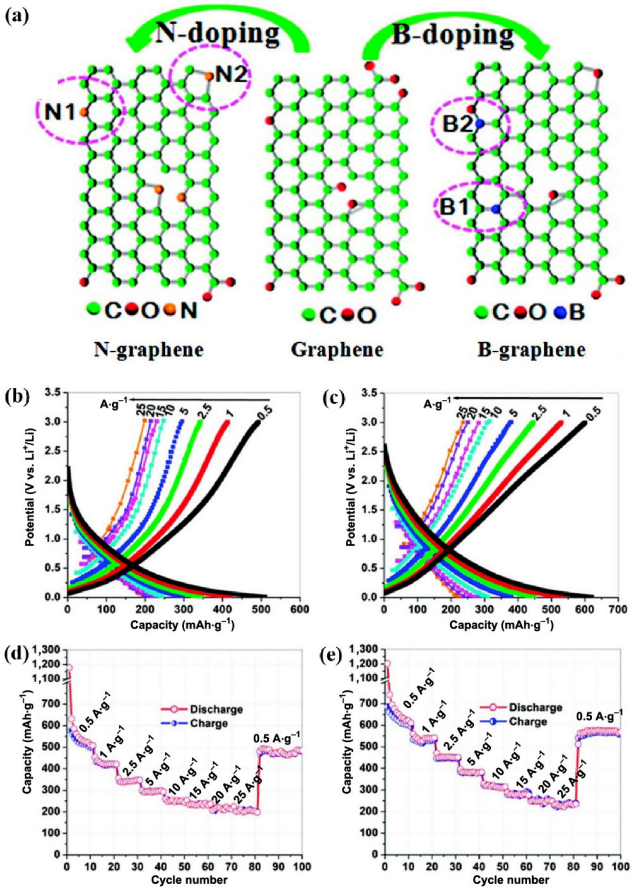

Figure 7 (a) Schematic structure of the binding conditions of N and B in a graphene lattice, highlighted by magenta dotted rings. Galvanostatic charge-discharge curves of (b) N-doped and (c) B-doped graphene electrodes at various current rates. Rate capabilities and cycle performance of (d) N-doped and (e) B-doped graphene electrodes at current densities from 0.5 to 25 A·g^{-1}. Reproduced with permission from Ref. [81], © American Chemical Society 2011.

charge transfer states for different N-existing forms and revealed that pyrrolic N sites showed higher efficiency for charge transfer, which caused the ultrafast lithium storage. Recently, Jianhua Tian et al. proposed a one-step facile calcination and activation process by using LiOH as Li source and activating agent to fabricate $Li_4Ti_5O_{12}$/N, S co-doped porous graphene composites [83]. Through DFT calculation, they elaborated that the N, S co-doped graphene exhibited a higher adsorption energy and lower diffusion activation energy of Li^+, facilitating the storage and transfer of Li^+ and thus the high rate capability.

3.3 Design and construction of graphene-based macroscopic architectures

In general, graphene usually tends to be in a random aggregation due to the π-π interaction and van der Waals force between layers. For applications in the lithium-ion batteries, such agglomeration will affect the demonstration of intrinsic properties of graphene, such as the high specific surface area and remarkable conductivities. Graphene macrostructures are macroscopic forms composed of graphene sheets assembled according to a certain structure and orientation, which not only tackle the random aggregation of graphene lamellae while maintain excellent physicochemical properties of graphene, but also possess controllable micro-nano structures. According to the structural forms, graphene macrostructures can be divided into three categories: 1D macrostructures, such as fibres and cables, 2D macrostructures, such as films and paper, and 3D macrostructures, such as hydrogel, foams and honeycomb-like structures, as indicated in Fig. 8 [84–90]. Due to the macroscopic morphology obtained by assembly, many properties can be obtained and utilized to enhance the efficiency of charge transport in LIBs, which can be summarized as the following advantages: 1) The large specific surface area of graphene-based macrostructures provide abundant electrochemical reaction interfaces for Li^+ storage; 2) The interconnected graphene lamellae within graphene-based macrostructures can construct efficient and continuous electronic conductive networks to collect/transport electrons from/to the active particles during the charge and discharge processes; 3) the rich pore structures formed from the interlinked graphene nanosheets allow for the penetration of electrolyte and provide short diffusion distances and multi-channels for ion transfer, effectively facilitating the diffusion of Li^+. For instance, Qian Cheng et al. reported a honeycomb-like porous graphene sponge additive prepared from chemically derived graphene sheets for both anode and cathode materials [91]. The charge capacity retention and cyclability at high rate improved greatly with the addition of porous graphene sponge additives, which was attributed to the excellent electric conductivity, high specific surface area, and high ability of electrolyte absorption of graphene sponge additives. Huiming Cheng et al. presented a template-directed CVD technique to synthesize 3D graphene foams which demonstrated outstanding electrical conductivity superior to that of macroscopic graphene from chemically derived graphene sheets due to the high quality of as-formed graphene sheets and their perfect connection in the 3D macrostructures [92].

The design and precise control of the pore structure in graphene-based macrostructures can be used for the optimization of charge transport to deliver high-rate energy storage at practical

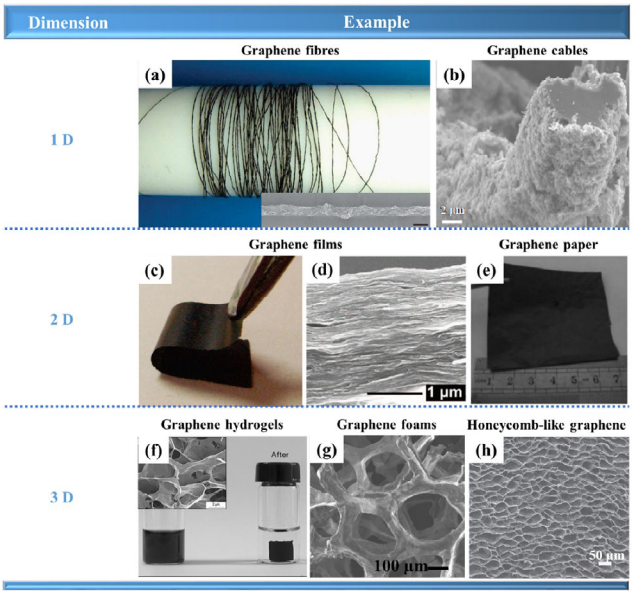

Figure 8 Schematic diagram of graphene-based macroscopic architectures in different dimensions. (a) and (b) Graphene-based 1D macroscopic forms. (a) Reproduced with permission from Ref. [84], © Zhen, X. et al. 2011. (b) Reproduced with permission from Ref. [85], © Elsevier Ltd. 2020. (c)–(e) Graphene-based 2D macroscopic forms. (c) and (d) Reproduced with permission from Ref. [86], © American Chemical Society 2008. (e) Reproduced with permission from Ref. [87], © WILEY-VCH Verlag GmbH & Co. KGaA, Weinheim, 2009. (f)–(h) Graphene-based 3D macroscopic forms. (f) Reproduced with permission from Ref. [88], © Institute of Coal Chemistry, Chinese Academy of Sciences. Published by Elsevier Limited. 2011. (g) Reproduced with permission from Ref. [89], © American Chemical Society 2013. (h) Reproduced with permission from Ref. [90], © Macmillan Publishers Limited. 2012.

levels of mass loading. As reported by Xiangfeng Duan et al., a 3D holey-graphene/niobia (Nb_2O_5) composite electrode with optimized porosity was obtain by oxidative-etching process, which achieved an optimized charge transport to deliver high areal capacity and high-rate capability at high mass loading (>10 mg·cm^{-2}). Such an ultrahigh-rate energy storage was due to the well-designed architecture with highly interconnected networks and hierarchical pores that produces interpenetrating electron transport and ion transport paths [93]. In spite of great progress achieved by porous graphene macrostructures to enhance the efficiency of charge transport in LIBs, they were normally loosely packed, which lead to the low utilization efficiency of pores and consequently a relatively low volumetric capacity. For this reason, Liangti Qu's group developed a one-pot hydrothermal process with subsequent vacuum drying and annealing treatment to prepare N-doped holey-graphene monolith (NHGM) with a dense microstructure and high density (Fig. 9) [94]. The highly compact but porous architecture of NHGM together with N doping gave rise to remarkable volumetric capacity and cycling stability at high mass loading which have rarely been reported yet.

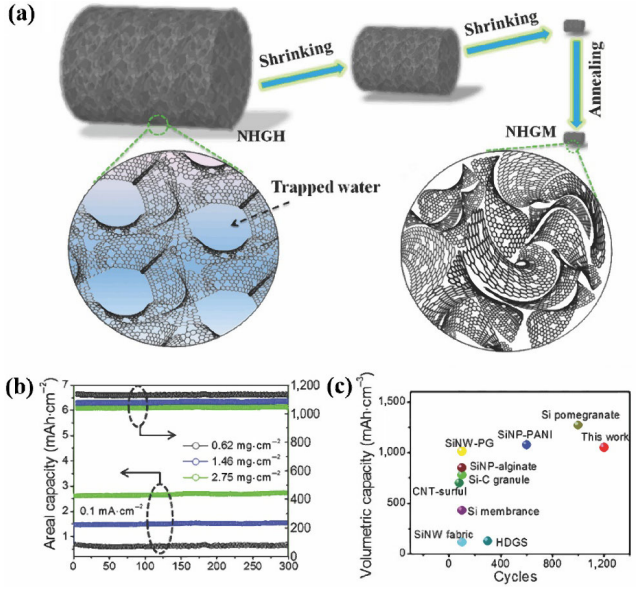

Figure 9 (a) Schematic illustration of the fabrication of NHGM. (b) Cycling performance of the NHGM electrode with different areal mass loadings. (c) Volumetric capacity versus cycle number for the NHGM electrode in comparison with other reported Si-based and carbon/sulfur hybrid electrodes. Reproduced with permission from Ref. [94], © WILEY-VCH Verlag GmbH & Co. KGaA, Weinheim 2016.

4 Application of graphene in regulating charge transport in LIBs

4.1 Graphene-based composites

Achieving high specific capacity at high rate (i.e., rate capability) is significantly important for practical application of LIBs, which promotes power performance [95, 96]. However, with inferior conductivity, the rate capability of various active materials could hardly meet the rapidly increasing market demands [97]. Assembling electroactive materials with a continuous and percolating electron- and ion-transport facilitator is essential to achieve high utilization at high rate, especially for those with intrinsically poor electronic and ionic conductivities [11]. Graphene, with high ionic mobility on the plane and ballistic electron transport [98, 99], tends to form a bi-continuous conductive network. Electroactive materials, either anchored, wrapped or encapsulated by graphene (Fig. 10) have been reported to exhibit superior rate ability [9, 100–107].

4.1.1 *Composites as cathode materials*

$LiFePO_4$, which has a high theoretical specific capacity of 170 mAh·g^{-1} and especially a superior safety performance but inherently poor conductivity, is a typical example. Studies show that $LiFePO_4$/graphene nanocomposite cathodes deliver highly improved electrochemical performance due to the effective electron transport promoted by graphene [108–110]. For instance, Ju-Won Jeon et al. constructed $LiFePO_4$/graphene hybrid cathodes for LIBs via facile water-processable and sprayable electrode fabrication methods which exhibited superior rate (37 mAh·g^{-1} at 2,040 mA·g^{-1}) and cycling performance (88% capacity retention after 1,000 cycles at 3,400 mA·g^{-1}) than conventional $LiFePO_4$-based electrodes [108]. Moreover, Gaixia Zhang et al. investigated graphene with different sizes and morphologies and proposed an optimized graphene content (1%) via tuning size and morphology of graphene [109].

Considering limited ion diffusion through the basal plane of perfect graphene [111], porous graphene with 3D network/aerogel structures were developed to afford rapid electron/ion transport to achieve higher rate capability, and excellent cycle stability in $LiFePO_4$, cathodes, especially at high loading [112]. For instance, Yingke Zhou's group synthesized a three-dimensional graphene aerogel supporting $LiFePO_4$ nanoparticles (LFP/GA) which demonstrated a high capacity of 167 mAh·g^{-1} at the rate of 0.1 C, and a remarkable rate capacity of ~ 120 mAh·g^{-1} at 10 C, superior to that of the graphene nanosheets supporting LFP due to the well-developed conductive network and aerogel structures which offer plenty of interconnected open pores for ion diffusion [112]. Heteroatom (N and B)-doped 3D porous graphene also attract much attention as heteroatoms promote both electron and ion transport for organic electrolyte-based LIBs [81, 113, 114]. As reported by Dianlong Wang et al., the $LiFePO_4$, in combination with N-doped graphene aerogels, displayed high rate capabilities (78 mAh·g^{-1} at 100 C) and excellent cycle stability, while the commercial LFP/C was almost un-rechargeable at relevant current rates [114]. In addition, homologous performance results are also observed in other active materials, such as $LiMn_{0.75}Fe_{0.25}PO_4$ [115], $Li_3V_2(PO_4)_3$ [116], $LiMn_2O_4$ [117], etc., the specific examples are listed in Table 2.

4.1.2 *Composites as anode materials*

Titanium oxides [118, 119] ($Li_4Ti_5O_{12}$ and TiO_2) based on insertion/de-insertion reaction, metal oxides/phoshides/sulfides/nitrides (M = Mn, Fe, Co, Ni, Cu, etc.) based on conversion reaction, and semimetals/oxides (Si, Ge, SiO_x, etc.) based on alloy/de-alloying reaction, the most promising anode materials for high energy density LIBs, also suffer sluggish charge transfer kinetics. It has been proved that combination with graphene is an effective way to improve electrochemical performance of these anode materials [83, 100, 105, 120–126]. Recently, Dongdong Wang et al. reported $Li_4Ti_5O_{12}$/nitrogen, sulfur co-doped porous graphene composites (LTO/N, S-PG). DFT calculations revealed that co-doped N and S atoms not only significantly facilitate Li^+ adsorption, but also ameliorate Li^+ diffusion in graphene. Furthermore, the synergistic effects of nanosized LTO and porous graphene endowed the composites with efficient Li^+ diffusion channels and electron-conductive networks. As a result, the LTO/N, S-PG delivered extraordinarily high rate capability (e.g., 130 mAh·g^{-1} at 80 C and 123 mAh·g^{-1} at 100 C), and excellent cycling stability (83.1% capacity retention after

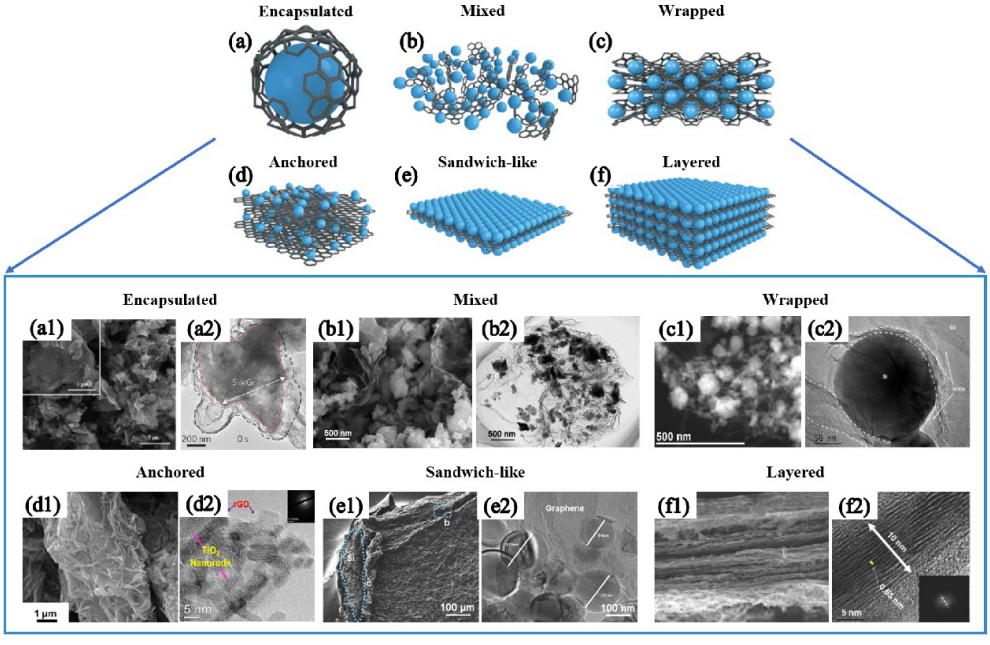

Figure 10 Structural models of graphene-based composites. Reproduced with permission from Ref. [6], © Elsevier Ltd. 2017. Encapsulated: Single active-material particles are encapsulated by graphene. Reproduced with permission from Ref. [100], © Macmillan Publishers Limited. 2016. Mixed: Graphene and active materials are synthesized separately and mixed mechanically during the electrode preparation. Reproduced with permission from Ref. [103], © Elsevier B.V. 2011. Wrapped: The active-material particles are wrapped by multiple graphene sheets. Reproduced with permission from Ref. [104], © American Chemical Society 2019. Anchored: This is the most common structure for graphene composites, in which electroactive nanoparticles are anchored to the graphene surface. Reproduced with permission from Ref. [105], © Elsevier B.V. 2019. Sandwich-like model: Graphene is used as a template to generate active material/graphene sandwich structures. Reproduced with permission from Ref. [106], © WILEY-VCH Verlag GmbH & Co. KGaA, Weinheim 2016. Layered model: Active-material nanoparticles are alternated with graphene sheets to form a composite layered structure. Reproduced with permission from Ref. [107], © The Electrochemical Society 2013.

4,000 cycles at 20 C). In addition, their superior electrochemical performance was also demonstrated in the full cells with $LiNi_{0.5}Mn_{1.5}O_4$ cathode, which displayed 89.5% capacity retention after 500 cycles at 5 C [83]. Li Li et al. successfully constructed 3D graphene-encapsulated Fe_3O_4 (3D Fe_3O_4@rGO) composite. The composite showed satisfactory cycling stability and a high capacity (665 mAh·g^{-1}) after 200 cycles even at 1,000 mAh·g^{-1} which was mainly ascribed to the flexible 3D rGO nanosheets that promoted both electron and Li^+ transport [126]. Impressively, Yi Cui's group encapsulated Si microparticles (1–3 μm) in conformally synthesized cages consisting of multilayered graphene (SiMP@Gr). The intrinsically high electronic conductivity and ionic permeability through defects of graphene cage guaranteed persistent electrochemical activity of SiMPs and the resulting fractured particles. As a result, cycle performance (over 85% capacity retention after 300 cycles) of SiMP@Gr at high rate far surpassed that of amorphous-carbon-coated SiMP [100]. Besides the above studies, some results with encouraging performance are described in Table 2 [83, 100, 102–108, 112, 114–117, 121–131].

Research shows that mass ratio of the graphene component in the composite is normally distributed in the range of > 10 wt.%, however, further optimization of the structural configuration and mass ratio distribution between graphene and the other active components are still critical issues that should be addressed to achieve better electrochemical performance in term of reversible capacity, rate performance, cycling life, etc.

4.2 Current collector

Current collectors (CC) are essential components to mechanically bridge the electrode materials and external circuit, which would substantially influence the overall performance of LIBs. However, commercial current collectors (Al foil and Cu foil for cathode and anode, respectively) have the following drawbacks: (1) high mass fraction (9 wt.%–10 wt.% of the total mass of the cell), which would severely reduce the energy densities of LIBs [132]; (2) large interfacial electric resistance resulting from the poor contact and weak adhesion between current collectors and electrode materials (Fig. 11(a)), which hampers the rate capability especially for flexible LIBs [133]. With high electrical conductivity, low mass density, and structural tunability, graphene has been widely reported as the free-standing CC or the conductive coating on the traditional CC for LIBs to achieve better wetting, stronger adhesion, greater mechanical durability, and lower contact resistance (Figs. 11(b)–11(e)).

4.2.1 *Free-standing current collector*

Graphene assembly structures have been reported as free-standing current collectors to replace metal foils [89, 93, 134, 136–139]. Recently, Zhongfan Liu's group demonstrated that the graphene film as the flexible current provided a satisfactory electrochemical performance in flexible LIBs based on the sufficient conductivity, strong adhesion, and strong mechanical flexibility. With $LiCoO_2$ and $Li_4Ti_5O_{12}$ serving as the cathode and the anode, respectively, the flexible graphene battery exhibited a good rate capability (143.0 mAh·g^{-1} at 1 C), stable cycle performance (no observed capacity loss after 100 thousand cycles of mechanical bending) and good safety. Besides, the mass energy density and power density are both 1.4 times higher than a standard electrode using metal foils as current collectors [136]. Owing to the well-developed electron/ion conductive networks, 3D graphene, as freestanding current collectors, contributed to the high rate capability even at high loading. Huiying Yang et al. developed a facile and general approach to obtain 3D interconnected porous nitrogen-doped graphene foam (NGF) with encapsulated Ge quantum dot/nitrogen-doped graphene yolk-shell nano architecture for high-performance LIBs (Fig. 11(c)), in which the NGF-based current collector

Table 2 Emerging performance of graphene-based composites for Li-ion batteries [83, 100, 102–108, 112, 114–117, 121–131]

Material type	Electrode type	Graphene amount	Performance	Ref.
$LiFePO_4$/graphene	Cathode	20 wt.%	37 mAh·g^{-1} at 2.04 A·g^{-1}; 26 mAh·g^{-1} (88% capacity retention) after 1,000th cycle at 3.4 A·g^{-1}	[108]
LFP@GA	Cathode	9.7 wt.%	~ 120 mAh·g^{-1} at 10 C; 88.5% capacity retention after 800th cycle at 1 C	[112]
LFP@N-GA	Cathode	15.36 wt.%	78 mAh·g^{-1} at 100 C; 86 mAh·g^{-1} (80% capacity retention) after 1,000th cycle at 10 C	[114]
$LiMn_{0.75}Fe_{0.25}PO_4$/rmGO	Cathode	20 wt.%	107 mAh·g^{-1} at 50 C; 98.1% capacity retention from the 11th to the 100th cycle at 0.5 C	[115]
$Li_3V_2(PO_4)_3$@NPCM@rGO	Cathode	NA[a]	~90 mAh·g^{-1} at 50 C; 88 mAh·g^{-1} after 1,000th cycle at 50 C	[116]
Spinel $LiMn_2O_4$/RGO	Cathode	27 wt.%	101 mAh·g^{-1} at 100 C; 96% capacity retention after 100th cycle at 50 C	[117]
LTO/N, S-PG	Anode	5.8 wt.%	130 mAh·g^{-1} at 80 C; 83.1% capacity retention after 4,000 cycles at 20 C	[83]
$Li_4Ti_5O_{12}$/holey-graphene	Anode	50 wt.%	98 mAh·cm^{-3} at 17.5 A·g^{-1};100.8 mAh·cm^{-3} (84% capacity retention) after 1,000th cycle at 7 A·g^{-1}	[127]
$Li_4Ti_5O_{12}$/graphene	Anode	5 wt.%	122 mAh·g^{-1} at 30 C; 124 mAh·g^{-1} (94.8% capacity retention) after 300th cycle at 20 C	[103]
R-TiO_2/rGO	Anode	7.4 wt.%	55 mAh·g^{-1} at 30 C; 96 mAh·g^{-1} after 1,000th cycle at 20 C	[105]
SA- TiO_2/RGO	Anode	10.7 wt.%	135 mAh·g^{-1} at 10 A·g^{-1}; 98 mAh·g^{-1} after 2,000th cycle at 5 A·g^{-1}	[128]
Co_3O_4/graphene	Anode	5.8 wt.%	509.3 mAh·g^{-1} at 5.62 C; 851.5 mAh·g^{-1} (92.1% capacity retention) after 2,000th cycle at 2.25 C	[122]
Graphene anchored with Co_3O_4	Anode	~ 24.6 wt.%	484 mAh·g^{-1} at 0.5 A·g^{-1}; 935 mAh·g^{-1} after 30 cycles at a specific current of 0.05 A·g^{-1}	[123]
Co_3O_4-graphene nanoflowers	Anode	NA	233 mAh·g^{-1} at 10 A·g^{-1}; 1,120.8 mAh·g^{-1} after 250 cycles at a specific current of 1 A·g^{-1}	[124]
FLG-anchored Fe_3O_4	Anode	26.6 wt.%	1,413 mAh·g^{-1} after 100 cycles at a specific current of 1 A·g^{-1};	[125]
3D Fe_3O_4@rGO	Anode	NA	712 mAh·g^{-1} at 3.2 A·g^{-1}; 1,139 mAh·g^{-1} (85% capacity retention) after 100th cycle at 0.4 A·g^{-1}	[126]
Silica-modified SnO_2-graphene "slime"	Anode	NA	802 mAh·g^{-1} at 2 A·g^{-1}; 1,950 mAh·g^{-1} after 1,000 cycles at a specific current of 0.5 A·g^{-1}	[121]
Graphene-MnO_2-GNRs	Anode	68 wt.%	~ 300 mAh·g^{-1} at 1 A·g^{-1}; 612 mAh·g^{-1} after 250th cycle at 0.4 A·g^{-1}	[129]
SiMP@Gr	Anode	9 wt.%	500 mAh·g^{-1} at 4 C; 1,400 mAh·g^{-1} (85% capacity retention) after 300th cycle at 0.5 C	[100]
Graphene bubble film/silicon composite	Anode	42 wt.%	900 mAh·g^{-1} at 3 A·g^{-1}; 1,325 mAh·g^{-1} after 100 cycles at 0.5 A·g^{-1}	[104]
Si@C-rGO	Anode	NA	767 mAh·g^{-1} at 3 A·g^{-1}; 600 mAh·g^{-1} after 100 cycles at a specific current of 1.5 A·g^{-1}	[106]
GrSiNPs	Anode	~ 47 wt.%	623 mAh·g^{-1} at 4 A·g^{-1}; 1,613 mAh·g^{-1} after 800th cycle at 0.4 A·g^{-1}	[130]
MoS_2@graphene	Anode	4.7 wt.%	570 mAh·g^{-1} at 1 A·g^{-1}; 894.1 mAh·g^{-1} after 100th cycle at 0.1 A·g^{-1}	[131]
MoS_2@rGO	Anode	~ 10.4 wt.%	935 mAh·g^{-1} at 5 A·g^{-1}; 1,345 mAh·g^{-1} after 400th cycle at 0.5 A·g^{-1}	[102]
MoS_2-graphene nanocomposites	Anode	~ 77.9 wt.%	500 mAh·g^{-1} at 2 A·g^{-1}; ~ 600 mAh·g^{-1} after 100th cycle at 0.5 A·g^{-1}	[107]

[a](NA): not found from the article.

with a continuous porous network is conducive to offer better electrical and electrolyte contact. As a result, the electrode delivered high specific reversible capacity (1,220 mAh·g^{-1}), long cycling capability (over 96% reversible capacity retention from the second to 1,000 cycles) and ultra-high rate performance (over 800 mAh·g^{-1} at 40 C) [134]. Considering the ion diffusion limitations in thicker electrodes, Xiangfeng Duan's group designed 3D holey-graphene backbone with tailored porosity to further promote ion transport. With optimized charge transport, 3D holey-graphene/Nb_2O_5 composite delivered high areal capacity (139 mAh·g^{-1}) at high-rate capability (10 C) and high mass loading (> 11 mg·cm^{-2}) [93].

4.2.2 *Coating on current collector*

Interface design between current collector and electroactive materials plays a key role in the charge transport for lithium-ion batteries. Graphene-coated metal foils as current collectors benefit rate capability as the graphene coating could effectively reduce interfacial electric resistance [133, 135, 140–142]. Recently, Hailin Peng et al. proved interfacial electric resistance dominates, i.e., ~ 2 orders of magnitude higher than that of electrode materials, through systematic quantitative studies of the interfacial properties. At the same time, the group decreased interfacial resistance greatly by fabricating graphene-coated Al foil as the current collector using plasma-enhanced chemical vapor deposition (Fig. 11(d)), wherein the graphene coating constructed a powerful electronic network between the current collector and electrode materials. The LFP electrodes on the graphene-coated Al current collector delivered a power density output of ~ 5,300 W·kg^{-1} at an energy density of ~ 220 Wh·kg^{-1}, whereas the LFP electrode on the Al current collector could deliver only ~ 3,700 W·kg^{-1} at ~ 21 Wh·kg^{-1} [133]. To achieve ultrafast cycling performances, Hyo-Jin Ahn's group emphasized the importance of high electrical conductivity of the coating layer on Al current collectors and successfully fabricated an N- and F-doped graphene interfacial layer on micropatterned Al foil using roll pressing and dip coating processes (Fig. 11(e)). With the doped N and F atoms in grapheme, the electrical conductivity, charge accessibility, and ion diffusion rate of the graphene were further improved. The cathode electrode fabricated with the resultant current collector exhibited ultrafast cycling stability at extremely high rate and long-term cycling performance

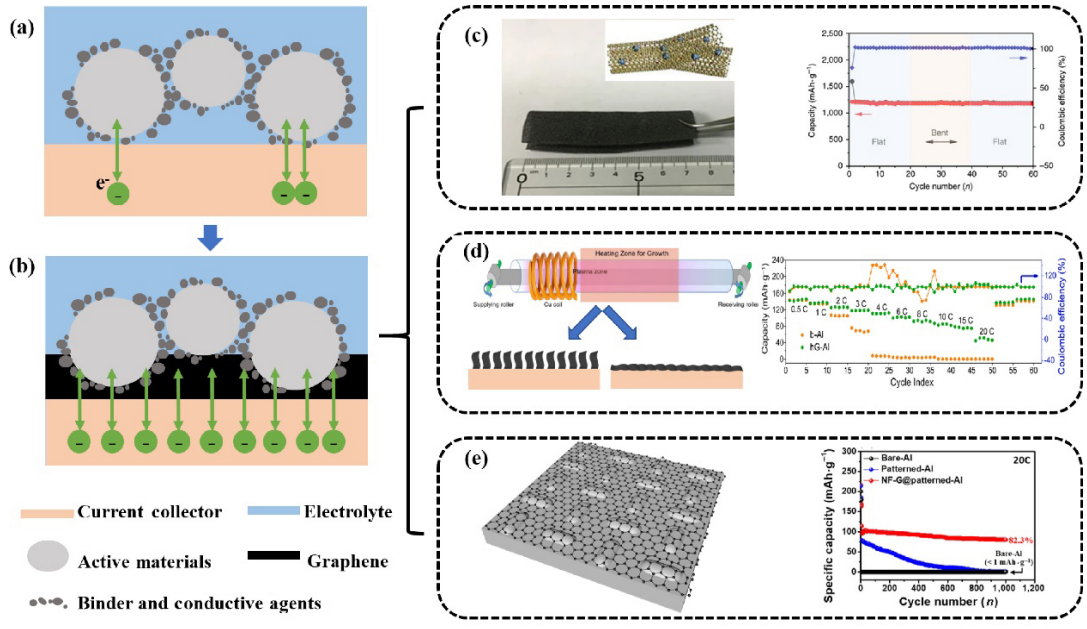

Figure 11 (a) Schematic illustration of interfacial electric resistance existing at the interface between current collectors and electrode materials due to the poor contacts and weak adhesions. (b) Schematic illustration of efficient electron transfer between graphene modified current collectors and electrode materials. Schematic structures and electrochemical characterizations of (c) 3D interconnected porous nitrogen-doped graphene foam as a current collector for flexible rechargeable LIB. Reproduced with permission from Ref. [134], © Mo, R. et al. 2017. (d) Graphene-coated Al foil as the current collector using plasma-enhanced chemical vapor deposition for LFP cathodes. Reproduced with permission from Ref. [133], © American Chemical Society 2020, and (e) N- and F-doped graphene interfacial layer on micropatterned Al foil using roll pressing and dip coating processes for NCA cathodes. Reproduced with permission from Ref. [135], © American Chemical Society 2020.

(specific capacity of 87.1 mAh·g^{-1} with capacity retention of 82.3% at 20 C after 1,000 cycles) [135]. Besides, Xiaofei Liu et al. replaced amorphous carbon with vertical graphene nanowalls as coating on Cu foil. As a result, it exhibited a good rate performance with ~ 190 mAh·g^{-1} at 3 C, in contrast with the commercial carbon-coated copper (~ 160 mAh·g^{-1}) and the traditional bare copper (~ 90 mAh·g^{-1}) [141].

4.3 Conductive agent

Conductive agents, constructing electron networks inside electrodes, play an important role in achieving high utilization of active materials. Compared with the "point-to-point" contact mode of carbon black (CB) and "line-to point" contact mode of CNTs, the "plane-to-point" contact mode of graphene is more advantageous for effective conductive network (Fig. 12(a)) [143–147]. Xufang Wei et al. reported improvement on the rate performance of $LiFePO_4$ cathodes using graphene as conductive agents (LFP/C-G). Compared with the conventional LFP/C-CB cathodes, LFP/C-G cathodes displayed better rate performance (~ 39 mAh·g^{-1}, 27 mAh·g^{-1} at 30 C for LFP/C-G, LFP/C-CB respectively) [144]. In addition, Dianlong Wang's group showed that graphene in comparison with CNTs and acetylene black (AB), as conductive agent (Fig. 12(b)) exhibited better rate performance in $LiFePO_4$ cathode [145]. Jang-Kyo Kim's group

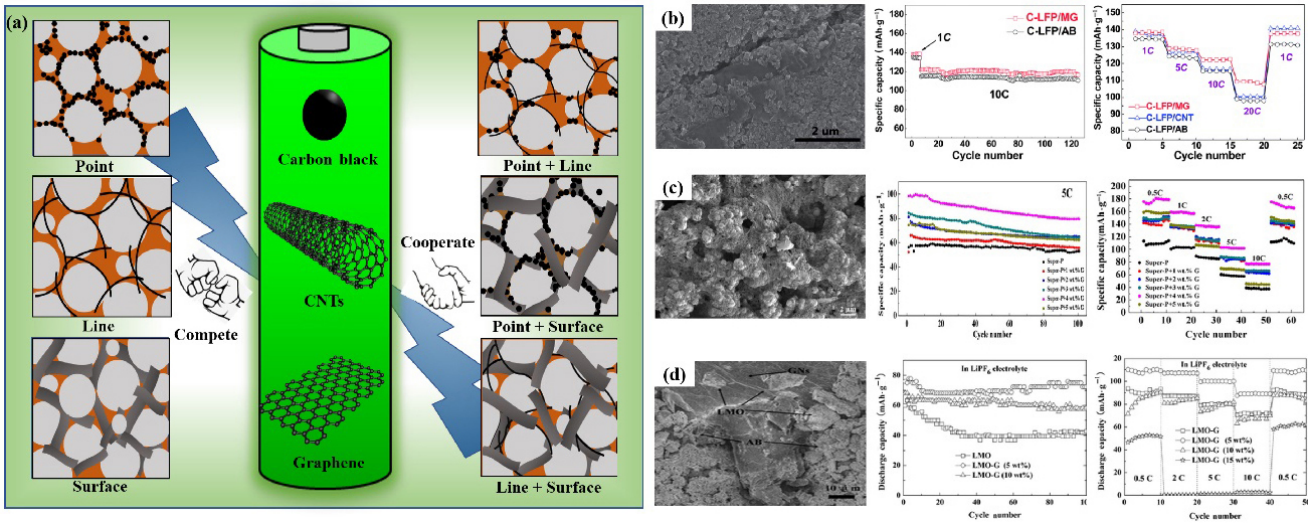

Figure 12 (a) Competition and cooperation of graphene with other conductive agents. Reproduced with permission from Ref. [149], © China Science Publishing & Media LTD 2020. Morphology and electrochemical characterizations of (b) LFP electrode with graphene conductive agent. Reproduced with permission from Ref. [145], © The Royal Society of Chemistry 2014. (c) Nb_2O_5 electrode with Super-P and graphene compound conductive agents. Reproduced with permission from Ref. [150], © Elsevier B.V. 2018, and (d) spinel $LiMn_2O_4$ electrode with acetylene black and graphene compound conductive agents. Reproduced with permission from Ref. [151], © The Royal Society of Chemistry 2013.

pointed out that both the size and thickness of graphene played an important role in determining the percolation threshold through a parametric study. Under this guidance, a percolation threshold of 1.8 wt.% of the graphene (a size of 46 μm and a thickness of 4.5 nm) was obtained for the $Li_4Ti_5O_{12}$ anodes, much lower than that of CB [148]. Studies also showed that the combination of graphene with other conductive agent generates synergistic effects and further improves the electronic conductivity and Li^+ transport throughout the entire electrode (Fig. 12(a)) [149–152]. Hongwen Chen et al. showed enhanced performance of Nb_2O_5 cathode with Super-P and graphene compounds as the conductive agents (Fig. 12(c)). The specific capacity of the battery with 4 wt.% graphene added rise up to 180 $mAh \cdot g^{-1}$ at the current rate of 0.5 C, as compared with the battery only using Super-P as conductive agent [150]. In addition, Houyi Ma's group observed that the specific capacity and cycling performance of $LiMn_2O_4$ (LMO) were enhanced significantly when graphene co-existed with AB at an appropriate weight ratio in the LMO-based electrode (Fig. 12(d)). The unusual phenomenon was attributed to the synergy effect between the "plane-to-point" conducting mode of graphene and the "filling" mode of AB, which greatly decreased the charge-transfer resistance of the LMO-based electrode [151]. Besides, there are reports involved in CNTs and graphene compounds as the binary conductive agents [153], even the ternary conductive agents consisting of CNTs, SP and graphene [154], which all exhibited superior performance than the individual conductive agents.

5 Summary and outlook

In this review, the recent progress on the structural design and interfacial modification strategies of graphene to regulate the charge transport in LIBs have been summarized. Besides, the structure-performance relationships between the structure of the graphene and its dedicated applications for LIBs have also been clarified in detail. Despite significant improvements made towards achieving fast charge transport to boost the battery performance, there still remain several issues to be addressed for the optimal use of graphene in LIBs.

First, considering that the electrochemical reaction of LIBs is influenced by both ion and electron transport, therefore, constructing highly efficient ionic and electronic conducting network is highly desirable, which requires further optimization of the structural configuration and mass ratio of graphene to active particles or to other conductive carbon components under the specific application system. However, systematic research on the synergistic effects between graphene and other components is still lacking which impedes the realization of both high electron and ion transfer.

Second, since the electronic conductivity of graphene mainly stems from its long-range π-conjugated structures, the oxygen functional groups on the plane play a major role in its conductivity, while functional groups attached to the edge exert less influence. Therefore, the precise control of the density and spatial distribution of oxygen functional groups in the graphene matrix are in favor of demonstrating the advantages of oxygen functional groups, like good wettability, while maintaining excellent conductivity. Nevertheless, such an accurate spatial control at atomic scale still remains a great challenge.

Third, modification by doping with N, S, B, and P to tailor the electronic property of graphene to enhance its storage capacity has also been attempted. Nevertheless, control over the doping type, level and configuration still remain great concerns, and advanced in situ characterization techniques are required to provide direct experimental evidence and fundamental understanding of the relevant effect on the properties of graphene.

Fourth, the abundant pore structure of graphene-based 3D macrostructures offers large specific surface area for lithium storage and multi-channels for ion transfer, resulting in a high gravimetric energy density. However, such porosity usually leads to a low packing density, and thus a low volumetric energy density. Although plenty of works have been dedicated to realizing the densification of porous graphene-based 3D macrostructures, the battery performance is still beyond satisfactory. Therefore, further optimization of the pore structure of graphene-based 3D macrostructures and realization of a tradeoff between the densification and porosity is desirable for achieving both high gravimetric and volumetric energy density for its commercial application in LIBs.

In summary, the excellent intrinsic properties, atomic structure tunability, and macrostructural constructability of graphene, make it a promising candidate for charge regulation in high-performance LIBs. Despite the intriguing battery performances achieved by graphene, the full demonstration of its potential in LIBs has not been realized yet. More efforts are required to address the issues with respect to the optimization of structural configuration and mass ratio of graphene to other materials, precise regulation of the distribution of oxygen functional groups, control over the doping type, level and configuration together with the tradeoff between the densification and porosity of graphene-based 3D macrostructures. Research on graphene in lithium batteries is expected to continue, with the promise of uncovering the mechanism of carbon-based nanomaterials in LIBs to revolutionizing lithium battery technology for practical applications.

Acknowledgements

The authors thank Shanshan Wang and Yangyong Sun from Peking university for their kind suggestions. This work was financially supported by the Ministry of Science and Technology of China (Nos. 2016YFA0200100 and 2018YFA0703502), the National Natural Science Foundation of China (Nos. 52021006, 51720105003, 21790052, and 21974004), the Strategic Priority Research Program of CAS (No. XDB36030100), and the Beijing National Laboratory for Molecular Sciences (No. BNLMS-CXTD-202001).

References

[1] Dominko, R.; Edström, K.; Fichtner, M.; Perraud, S.; Punckt, C.; Asinari, P.; Castelli, I. E.; Chistensen, R.; Clark, S.; Grimaud, A. et al. *BATTERY 2030+ Roadmap* [online]. 2020; https://battery2030.eu/digitalAssets/860/c_860904-l_1-k_roadmap-27-march.pdf (accessed Mar 2020).

[2] Liu, C.; Li, F.; Ma, L. P.; Cheng, H. M. Advanced materials for energy storage. *Adv. Mater.* **2010**, *22*, E28–E28.

[3] Bruce, P. G.; Scrosati, B.; Tarascon, J. M. Nanomaterials for rechargeable lithium batteries. *Angew. Chem., Int. Ed.* **2008**, *47*, 2930–2946.

[4] Gong, C. L.; Xue, Z. G.; Wen, S.; Ye, Y. S.; Xie, X. L. Advanced carbon materials/olivine $LiFePO_4$ composites cathode for lithium ion batteries. *J. Power Sources* **2016**, *318*, 93–112.

[5] Hu, L. H.; Wu, F. Y.; Lin, C. T.; Khlobystov, A. N.; Li, L. J. Graphene-modified $LiFePO_4$ cathode for lithium ion battery beyond theoretical capacity. *Nat. Commun.* **2013**, *4*, 1687.

[6] Qiao, Y. Q.; Feng, W. L.; Li, J.; Shen, T. D. Ultralong cycling stability of carbon-nanotube/$LiFePO_4$ nanocomposites as electrode materials for lithium-ion batteries. *Electrochim. Acta* **2017**, *232*, 323–331.

[7] Liu, N.; Lu, Z. D.; Zhao, J.; McDowell, M. T.; Lee, H. W.; Zhao, W. T.; Cui, Y. A pomegranate-inspired nanoscale design for large-volume-change lithium battery anodes. *Nat. Nanotechnol.* **2014**, *9*, 187–192.

[8] Liu, Y. P.; He, X. Y.; Hanlon, D.; Harvey, A.; Khan, U.; Li, Y. G.; Coleman, J. N. Electrical, mechanical, and capacity percolation leads to high-performance MoS_2/nanotube composite lithium ion battery electrodes. *ACS Nano* **2016**, *10*, 5980–5990.

[9] Raccichini, R.; Varzi, A.; Passerini, S.; Scrosati, B. The role of graphene for electrochemical energy storage. *Nat. Mater.* **2015**, *14*, 271–279.

[10] Wang, G. X.; Shen, X. P.; Yao, J.; Park, J. Graphene nanosheets for enhanced lithium storage in lithium ion batteries. *Carbon* **2009**, *47*, 2049–2053.

[11] Fang, R. P.; Chen, K.; Yin, L. C.; Sun, Z. H.; Li, F.; Cheng, H. M. The regulating role of carbon nanotubes and graphene in lithium-ion and lithium-sulfur batteries. *Adv. Mater.* **2019**, *31*, 1800863.

[12] Palacín, M. R.; de Guibert, A. Why do batteries fail? *Science* **2016**, *351*, 1253292.

[13] Padhi, A. K.; Nanjundaswamy, K. S.; Goodenough, J. B. Phospho-olivines as positive-electrode materials for rechargeable lithium batteries. *J. Electrochem. Soc.* **1997**, *144*, 1188–1194.

[14] Yuan, W. Y.; Zhang, Y. N.; Cheng, L. F.; Wu, H.; Zheng, L. X.; Zhao, D. L. The applications of carbon nanotubes and graphene in advanced rechargeable lithium batteries. *J. Mater. Chem. A* **2016**, *4*, 8932–8951.

[15] Bard, A. J.; Faulkner, L. R. *Electrochemical Methods*: *Fundamentals and Applications*; 2nd ed. Wiley: New York, 2001.

[16] Bazant, M. Z. Theory of chemical kinetics and charge transfer based on nonequilibrium thermodynamics. *Acc. Chem. Res.* **2013**, *46*, 1144–1160.

[17] Linden, D.; Reddy, T. B. *Handbook of Batteries*; 3rd ed. McGraw-Hill: New York, 2001.

[18] Winter, M.; Brodd, R. J. What are batteries, fuel cells, and super-capacitors? *Chem. Rev.* **2004**, *104*, 4245–4269.

[19] Delacourt, C.; Laffont, L.; Bouchet, R.; Wurm, C.; Leriche, J. B.; Morcrette, M.; Tarascon, J. M.; Masquelier, C. Toward understanding of electrical limitations (electronic, ionic) in $LiMPO_4$ (M = Fe, Mn) electrode materials. *J. Electrochem. Soc.* **2005**, *152*, A913–A921.

[20] Kaneko, M.; Nakayama, M.; Wakizaka, Y.; Kanamura, K.; Wakihara, M. Enhancement of electrochemical ion/electron-transfer reaction at solid|liquid interface by polymer coating on solid surface. *Electrochim. Acta* **2008**, *53*, 8196–8202.

[21] Park, M.; Zhang, X. C.; Chung, M.; Less, G. B.; Sastry, A. M. A review of conduction phenomena in Li-ion batteries. *J. Power Sources* **2010**, *195*, 7904–7929.

[22] Griffiths, D. J. *Introduction to Quantum Mechanics*; 2nd ed. Pearson Prentice Hall: Upper Saddle River, 2005.

[23] Datta, S. *Quantum Transport*: *Atom to Transistor*; Cambridge University Press: Cambridge, 2005.

[24] Kittel, C. *Introduction to Solid State Physics*; 7th ed. John & Wiley: New York, 1996.

[25] Callister, W. D. Jr. *Materials Science and Engineering*: *An Introduction*; 4th ed. Wiley: New York, 1997.

[26] Novoselov, K. S.; Geim, A. K.; Morozov, S. V.; Jiang, D.; Zhang, Y.; Dubonos, S. V.; Grigorieva, I. V.; Firsov, A. A. Electric field effect in atomically thin carbon films. *Science* **2004**, *306*, 666–669.

[27] Ashuri, M.; He, Q. R.; Shaw, L. L. Silicon as a potential anode material for Li-ion batteries: Where size, geometry and structure matter. *Nanoscale* **2016**, *8*, 74–103.

[28] Shi, S. Q.; Ouyang, C. Y.; Lei, M. S.; Tang, W. H. Effect of Mg-doping on the structural and electronic properties of $LiCoO_2$: A first-principles investigation. *J. Power Sources* **2007**, *171*, 908–912.

[29] Marzec, J.; Świerczek, K.; Przewoźnik, J.; Molenda, J.; Simon, D. R.; Kelder, E. M.; Schoonman, J. Conduction mechanism in operating a $LiMn_2O_4$ cathode. *Solid State Ionics* **2002**, *146*, 225–237.

[30] Cheng, F. Y.; Liang, J.; Tao, Z. L.; Chen, J. Functional materials for rechargeable batteries. *Adv. Mater.* **2011**, *23*, 1695–1715.

[31] Nitta, N.; Wu, F. X.; Lee, J. T.; Yushin, G. Li-ion battery materials: Present and future. *Mater. Today* **2015**, *18*, 252–264.

[32] Holm, R. *Electric Contacts: Theory and Application*. Springer: Heidelberg, 1967.

[33] Taheri, P.; Hsieh, S.; Bahrami, M. Investigating electrical contact resistance losses in lithium-ion battery assemblies for hybrid and electric vehicles. *J. Power Sources* **2011**, *196*, 6525–6533.

[34] Pandolfo, A. G.; Hollenkamp, A. F. Carbon properties and their role in supercapacitors. *J. Power Sources* **2006**, *157*, 11–27.

[35] Wilkinson, D. S. *Mass Transport in Solids and Fluids*; Cambridge University Press: Cambridge, 2000.

[36] Mehrer, H. *Diffusion in Solids*: *Fundamentals*, *Methods*, *Materials*, *Diffusion-Controlled Processes*; Springer-Verlag: Berlin, 2007.

[37] Uthaisar, C.; Barone, V. Edge effects on the characteristics of Li diffusion in graphene. *Nano Lett.* **2010**, *10*, 2838–2842.

[38] Han, S.; Wu, D. Q.; Li, S.; Zhang, F.; Feng, X. L. Graphene: A two-dimensional platform for lithium storage. *Small* **2013**, *9*, 1173–1187.

[39] Liu, T.; Sun, S. M.; Zang, Z.; Li, X. C.; Sun, X. L.; Cao, F. T.; Wu, J. F. Effects of graphene with different sizes as conductive additives on the electrochemical performance of a $LiFePO_4$ cathode. *RSC Adv.* **2017**, *7*, 20882–20887.

[40] Shida, K.; Sahara, R.; Mizuseki, H.; Kawazoe, Y. Controlling 3D percolation threshold of conductor-insulator composites by changing the granular size of conductors. *Mater. Trans.* **2011**, *52*, 2216–2219.

[41] Ma, X. L.; Ning, G. Q.; Sun, Y. Z.; Pu, Y. J.; Gao, J. S. High capacity Li storage in sulfur and nitrogen dual-doped graphene networks. *Carbon* **2014**, *79*, 310–320.

[42] Li, Q.; Tian, X. J.; Chen, Z.; Wu, J. Y.; Li, Y.; Li, Y. F. Synergistic effect of size distribution on the electrical and thermal conductivities of graphene-based paper. *J. Mater. Sci.* **2018**, *53*, 10261–10269.

[43] Tang, R.; Yun, Q. B.; Lv, W.; He, Y. B.; You, C. H.; Su, F. Y.; Ke, L.; Li, B. H.; Kang, F. Y.; Yang, Q. H. How a very trace amount of graphene additive works for constructing an efficient conductive network in $LiCoO_2$-based lithium-ion batteries. *Carbon* **2016**, *103*, 356–362.

[44] Cong, H. P.; Ren, X. C.; Wang, P.; Yu, S. H. Flexible graphene-polyaniline composite paper for high-performance supercapacitor. *Energy Environ. Sci.* **2013**, *6*, 1185–1191.

[45] Reddy, A. L. M.; Srivastava, A.; Gowda, S. R.; Gullapalli, H.; Dubey, M.; Ajayan, P. M. Synthesis of nitrogen-doped graphene films for lithium battery application. *ACS Nano* **2010**, *4*, 6337–6342.

[46] Luo, B.; Wang, B.; Li, X. L.; Jia, Y. Y.; Liang, M. H.; Zhi, L. J. Graphene-confined Sn nanosheets with enhanced lithium storage capability. *Adv. Mater.* **2012**, *24*, 3538–3543.

[47] Georgiou, T.; Jalil, R.; Belle, B. D.; Britnell, L.; Gorbachev, R. V.; Morozov, S. V.; Kim, Y. J.; Gholinia, A.; Haigh, S. J.; Makarovsky, O. et al. Vertical field-effect transistor based on graphene-WS_2 heterostructures for flexible and transparent electronics. *Nat. Nanotechnol.* **2013**, *8*, 100–103.

[48] Lee, S. K.; Jang, H. Y.; Jang, S.; Choi, E.; Hong, B. H.; Lee, J.; Park, S.; Ahn, J. H. All graphene-based thin film transistors on flexible plastic substrates. *Nano Lett.* **2012**, *12*, 3472–3476.

[49] Datta, D.; Li, J. W.; Koratkar, N.; Shenoy, V. B. Enhanced lithiation in defective graphene. *Carbon* **2014**, *80*, 305–310.

[50] Yu, Y. Z.; Guo, J. G.; Zhou, L. J. Theoretical investigation on the adsorption and diffusion of lithium-ion on and between graphene layers with size and defect effects. *Adsorpt. Sci. Technol.* **2016**, *34*, 212–226.

[51] Zhang, Y.; Hao, H. L.; Wang, L. L. Effect of morphology and defect density on electron transfer of electrochemically reduced graphene oxide. *Appl. Surf. Sci.* **2016**, *390*, 385–392.

[52] Banhart, F.; Kotakoski, J.; Krasheninnikov, A. V. Structural defects in graphene. *ACS Nano* **2011**, *5*, 26–41.

[53] Compagnini, G.; Giannazzo, F.; Sonde, S.; Raineri, V.; Rimini, E. Ion irradiation and defect formation in single layer graphene. *Carbon* **2009**, *47*, 3201–3207.

[54] Cruz-Silva, E.; Botello-Méndez, A. R.; Barnett, Z. M.; Jia, X.; Dresselhaus, M. S.; Terrones, H.; Terrones, M.; Sumpter, B. G.; Meunier, V. Controlling edge morphology in graphene layers using electron irradiation: From sharp atomic edges to coalesced layers forming loops. *Phys. Rev. Lett.* **2010**, *105*, 045501.

[55] Lin, Y.; Watson, K. A.; Kim, J. W.; Baggett, D. W.; Working, D. C.; Connell, J. W. Bulk preparation of holey graphene via controlled catalytic oxidation. *Nanoscale* **2013**, *5*, 7814–7824.

[56] Robertson, A. W.; Allen, C. S.; Wu, Y. A.; He, K.; Olivier, J.; Neethling, J.; Kirkland, A. I.; Warner, J. H. Spatial control of defect

creation in graphene at the nanoscale. *Nat. Commun.* **2012**, *3*, 1144.
[57] Zhong, J. H.; Zhang, J.; Jin, X.; Liu J. Y.; Li, Q. Y.; Li, M. H.; Cai, W. W.; Wu, D. Y.; Zhan, D. P.; Ren, B. Quantitative correlation between defect density and heterogeneous electron transfer rate of single layer graphene. *J. Am. Chem. Soc.* **2014**, *136*, 16609–16617.
[58] Du, Z. Z.; Ai, W.; Sun, C. C.; Zou, C. J.; Zhao, J. F.; Chen, Y.; Dong, X. C.; Liu, J. Q.; Sun, G. Z.; Yu, T. et al. Engineering the Li storage properties of graphene anodes: Defect evolution and pore structure regulation. *ACS Appl. Mater. Interfaces* **2016**, *8*, 33712–33722.
[59] Datta, D.; Li, J. W.; Shenoy, V. B. Defective graphene as a high-capacity anode material for Na- and Ca-ion batteries. *ACS Appl. Mater. Interfaces* **2014**, *6*, 1788–1795.
[60] Pang, Z. Q.; Shi, X. H.; Wei, Y. J.; Fang, D. N. Grain boundary and curvature enhanced lithium adsorption on carbon. *Carbon* **2016**, *107*, 557–563.
[61] Das, D.; Kim, S.; Lee, K. R.; Singh, A. K. Li diffusion through doped and defected graphene. *Phys. Chem. Chem. Phys.* **2013**, *15*, 15128–15134.
[62] Zhao, X.; Hayner, C. M.; Kung, M. C.; Kung, H. H. In-plane vacancy-enabled high-power Si-graphene composite electrode for lithium-ion batteries. *Adv. Energy Mater.* **2011**, *1*, 1079–1084.
[63] Chen, K. F.; Song, S. Y.; Liu, F.; Xue, D. F. Structural design of graphene for use in electrochemical energy storage devices. *Chem. Soc. Rev.* **2015**, *44*, 6230–6257.
[64] Ding, D.; Maeyoshi, Y.; Kubota, M.; Wakasugi, J.; Kanamura, K.; Abe, H. Holey reduced graphene oxide/carbon nanotube/$LiMn_{0.7}Fe_{0.3}PO_4$ composite cathode for high-performance lithium batteries. *J. Power Sources* **2020**, *449*, 227553.
[65] Deng, B. W.; Xu, R.; Wang, X. K.; An, L. C.; Zhao, K. J.; Cheng, G. J. Roll to roll manufacturing of fast charging, mechanically robust 0D/2D nanolayered Si-graphene anode with well-interfaced and defect engineered structures. *Energy Storage Mater.* **2019**, *22*, 450–460.
[66] Yan, L.; Zheng, Y. B.; Zhao, F.; Li, S. J.; Gao, X. F.; Xu, B. Q.; Weiss, P. S.; Zhao, Y. L. Chemistry and physics of a single atomic layer: Strategies and challenges for functionalization of graphene and graphene-based materials. *Chem. Soc. Rev.* **2012**, *41*, 97–114.
[67] Whitby, R. L. D. Chemical control of graphene architecture: Tailoring shape and properties. *ACS Nano* **2014**, *8*, 9733–9754.
[68] David, L.; Bhandavat, R.; Singh, G. MoS_2/graphene composite paper for sodium-ion battery electrodes. *ACS Nano* **2014**, *8*, 1759–1770.
[69] Chen, W. F.; Li, S. R.; Chen, C. H.; Yan, L. F. Self-assembly and embedding of nanoparticles by *in situ* reduced graphene for preparation of a 3D graphene/nanoparticle aerogel. *Adv. Mater.* **2011**, *23*, 5679–5683.
[70] Ha, S. H.; Lee, Y. J. Core-shell $LiFePO_4$/carbon-coated reduced graphene oxide hybrids for high-power lithium-ion battery cathodes. *Chem. –Eur. J.* **2015**, *21*, 2132–2138.
[71] Liu, L.; Gao, R.; Sun, L. M.; Han, S. B.; Chen, D. F.; Hu, Z. B.; Liu, X. F. Ultrahigh cycling stability and rate capability of $ZnFe_2O_4$@graphene hybrid anode prepared through a facile syn-graphenization strategy. *New J. Chem.* **2016**, *40*, 3139–3146.
[72] Kaiser, A. B. Electronic transport properties of conducting polymers and carbon nanotubes. *Rep. Prog. Phys.* **2001**, *64*, 1–49.
[73] Zhao, J. P.; Pei, S. F.; Ren, W. C.; Gao, L. B.; Cheng, H. M. Efficient preparation of large-area graphene oxide sheets for transparent conductive films. *ACS Nano* **2010**, *4*, 5245–5252.
[74] Becerril, H. A.; Mao, J.; Liu, Z. F.; Stoltenberg, R. M.; Bao, Z. N.; Chen, Y. S. Evaluation of solution-processed reduced graphene oxide films as transparent conductors. *ACS Nano* **2008**, *2*, 463–470.
[75] Li, D.; Müller, M. B.; Gilje, S.; Kaner, R. B.; Wallace, G. G. Processable aqueous dispersions of graphene nanosheets. *Nat. Nanotechnol.* **2008**, *3*, 101–105.
[76] Youn, H. C.; Bak, S. M.; Kim, M. S.; Jaye, C.; Fischer, D. A.; Lee, C. W.; Yang, X. Q.; Roh, K. C.; Kim, K. B. High-surface-area nitrogen-doped reduced graphene oxide for electric double-layer capacitors. *ChemSusChem* **2015**, *8*, 1875–1884.
[77] López, V.; Sundaram, R. S.; Gómez-Navarro, C.; Olea, D.; Burghard, M.; Gómez-Herrero, J.; Zamora, F.; Kern, K. Chemical vapor deposition repair of graphene oxide: A route to highly-conductive graphene monolayers. *Adv. Mater.* **2009**, *21*, 4683–4686.
[78] Dai, B. Y.; Fu, L.; Liao, L.; Liu, N.; Yan, K.; Chen, Y. S.; Liu, Z. F. High-quality single-layer graphene via reparative reduction of graphene oxide. *Nano Res.* **2011**, *4*, 434–439.
[79] Du, M.; Sun, J.; Chang, J.; Yang, F.; Shi, L. J.; Gao, L. Synthesis of nitrogen-doped reduced graphene oxide directly from nitrogen-doped graphene oxide as a high-performance lithium ion battery anode. *RSC Adv.* **2014**, *4*, 42412–42417.
[80] Cai, D. D.; Wang, S. Q.; Lian, P. C.; Zhu, X. F.; Li, D. D.; Yang, W. S.; Wang, H. H. Superhigh capacity and rate capability of high-level nitrogen-doped graphene sheets as anode materials for lithium-ion batteries. *Electrochim. Acta* **2013**, *90*, 492–497.
[81] Wu, Z. S.; Ren, W. C.; Xu, L.; Li, F.; Cheng, H. M. Doped graphene sheets as anode materials with superhigh rate and large capacity for lithium ion batteries. *ACS Nano* **2011**, *5*, 5463–5471.
[82] Wang, X.; Weng, Q. H.; Liu, X. Z.; Wang, X. B.; Tang, D. M.; Tian, W.; Zhang, C.; Yi, W.; Liu, D. Q.; Bando, Y. et al. Atomistic origins of high rate capability and capacity of N-doped graphene for lithium storage. *Nano Lett.* **2014**, *14*, 1164–1171.
[83] Wang, D. D.; Liu, H. X.; Shan, Z. Q.; Xia, D. W.; Na, R.; Liu, H. D.; Wang, B. H.; Tian, J. H. Nitrogen, sulfur co-doped porous graphene boosting $Li_4Ti_5O_{12}$ anode performance for high-rate and long-life lithium ion batteries. *Energy Storage Mater.* **2020**, *27*, 387–395.
[84] Xu, Z.; Gao, C. Graphene chiral liquid crystals and macroscopic assembled fibres. *Nat. Commun.* **2011**, *2*, 571.
[85] Zhao, Z.; Wang, J.; Cheng, M.; Wu, J.; Zhang, Q.; Liu, X. T.; Wang, C. W.; Wang, J. Y.; Li, K. X.; Wang, J. Z. N-doped porous carbon-graphene cables synthesized for self-standing cathode and anode hosts of Li-S batteries. *Electrochim. Acta* **2020**, *349*, 136231.
[86] Xu, Y. X.; Bai, H.; Lu, G. W.; Li, C.; Shi, G. Q. Flexible graphene films via the filtration of water-soluble noncovalent functionalized graphene sheets. *J. Am. Chem. Soc.* **2008**, *130*, 5856–5857.
[87] Chen, C. M.; Yang, Q. H.; Yang, Y. G.; Lv, W.; Wen, Y. F.; Hou, P. X.; Wang, M. Z.; Cheng, H. M. Self-assembled free-standing graphite oxide membrane. *Adv. Mater.* **2009**, *21*, 3007–3011.
[88] Sheng, K. X.; Xu, Y. X.; Li, C.; Shi, G. Q. High-performance self-assembled graphene hydrogels prepared by chemical reduction of graphene oxide. *New Carbon Mater.* **2011**, *26*, 9–15.
[89] Luo, J. S.; Liu, J. L.; Zeng, Z. Y.; Ng, C. F.; Ma, L. J.; Zhang, H.; Lin, J. Y.; Shen, Z. X.; Fan, H. J. Three-dimensional graphene foam supported Fe_3O_4 lithium battery anodes with long cycle life and high rate capability. *Nano Lett.* **2013**, *13*, 6136–6143.
[90] Qiu, L.; Liu, J. Z.; Chang, S. L. Y.; Wu, Y. Z.; Li, D. Biomimetic superelastic graphene-based cellular monoliths. *Nat. Commun.* **2012**, *3*, 1241.
[91] Cheng, Q. Porous graphene sponge additives for lithium ion batteries with excellent rate capability. *Sci. Rep.* **2017**, *7*, 925.
[92] Chen, Z. P.; Ren, W. C.; Gao, L. B.; Liu, B. L.; Pei, S. F.; Cheng, H. M. Three-dimensional flexible and conductive interconnected graphene networks grown by chemical vapour deposition. *Nat. Mater.* **2011**, *10*, 424–428.
[93] Sun, H. T.; Mei, L.; Liang, J. F.; Zhao, Z. P.; Lee, C.; Fei, H. L.; Ding, M. N.; Lau, J.; Li, M. F.; Wang, C. et al. Three-dimensional holey-graphene/niobia composite architectures for ultrahigh-rate energy storage. *Science* **2017**, *356*, 599–604.
[94] Wang, X. P.; Lv, L. X.; Cheng, Z. H.; Gao, J.; Dong, L. Y.; Hu, C. G.; Qu, L. T. High-density monolith of N-doped holey graphene for ultrahigh volumetric capacity of Li-ion batteries. *Adv. Energy Mater.* **2016**, *6*, 1502100.
[95] Schmuch, R.; Wagner, R.; Hörpel, G.; Placke, T.; Winter, M. Performance and cost of materials for lithium-based rechargeable automotive batteries. *Nat. Energy* **2018**, *3*, 267–278.
[96] Armand, M.; Tarascon, J. M. Building better batteries. *Nature* **2008**, *451*, 652–657.
[97] Liu, Y. Y.; Zhu, Y. Y.; Cui, Y. Challenges and opportunities towards fast-charging battery materials. *Nat. Energy* **2019**, *4*, 540–550.
[98] Bolotin, K. I.; Sikes, K. J.; Jiang, Z.; Klima, M.; Fudenberg, G.; Hone, J.; Kim, P.; Stormer, H. L. Ultrahigh electron mobility in suspended graphene. *Solid State Commun.* **2008**, *146*, 351–355.
[99] Heersche, H. B.; Jarillo-Herrero, P.; Oostinga, J. B.; Vandersypen, L. M. K.; Morpurgo, A. F. Bipolar supercurrent in graphene. *Nature* **2007**, *446*, 56–59.

[100] Li, Y. Z.; Yan, K.; Lee, H. W.; Lu, Z. D.; Liu, N.; Cui, Y. Growth of conformal graphene cages on micrometre-sized silicon particles as stable battery anodes. *Nat. Energy* **2016**, *1*, 15029.
[101] Xu, Q.; Sun, J. K.; Yu, Z. L.; Yin, Y. X.; Xin, S.; Yu, S. H.; Guo, Y. G. SiO_x encapsulated in graphene bubble film: An ultrastable Li-ion battery anode. *Adv. Mater.* **2018**, *30*, 1707430.
[102] Huang, J. R.; Liu, D. X.; Gu, C. P.; Liu, J. Y. General approach for preparing sandwich-structured metal sulfide@reduced graphene oxide as highly reversible Li-ion battery anode. *Mater. Res. Lett.* **2018**, *6*, 307–313.
[103] Shi, Y.; Wen, L.; Li, F.; Cheng, H. M. Nanosized $Li_4Ti_5O_{12}$/graphene hybrid materials with low polarization for high rate lithium ion batteries. *J. Power Sources* **2011**, *196*, 8610–8617.
[104] Wasalathilake, K. C.; Hapuarachchi, S. N. S.; Zhao, Y. B.; Fernando, J. F. S.; Chen, H.; Nerkar, J. Y.; Golberg, D.; Zhang, S. Q.; Yan, C. Unveiling the working mechanism of graphene bubble film/silicon composite anodes in Li-ion batteries: from experiment to modeling. *ACS Appl. Energy Mater.* **2020**, *3*, 521–531.
[105] Fu, Y. X.; Dai, Y.; Pei, X. Y.; Lyu, S. S.; Heng, Y.; Mo, D. C. TiO_2 nanorods anchor on reduced graphene oxide (R-TiO_2/rGO) composite as anode for high performance lithium-ion batteries. *Appl. Surf. Sci.* **2019**, *497*, 143553.
[106] Agyeman, D. A.; Song, K.; Lee, G. H.; Park, M.; Kang, Y. M. Carbon-coated Si nanoparticles anchored between reduced graphene oxides as an extremely reversible anode material for high energy-density Li-ion battery. *Adv. Energy Mater.* **2016**, *6*, 1600904.
[107] Hu, Y. H.; Li, X. F.; Lushington, A.; Cai, M.; Geng, D. S.; Banis, M. N.; Li, R. Y.; Sun, X. L. Fabrication of MoS_2-graphene nanocomposites by layer-by-layer manipulation for high-performance lithium ion battery anodes. *ECS J. Solid State Sci. Technol.* **2013**, *2*, M3034–M3039.
[108] Jeon, J. W.; Biswas, M. C.; Patton, C. L.; Wujcik, E. K. Water-processable, sprayable $LiFePO_4$/graphene hybrid cathodes for high-power lithium ion batteries. *J. Ind. Eng. Chem.* **2020**, *84*, 72–81.
[109] Fu, Y. Q.; Wei, Q. L.; Zhang, G. X.; Zhong, Y.; Moghimian, N.; Tong, X.; Sun, S. H. $LiFePO_4$-graphene composites as high-performance cathodes for lithium-ion batteries: The impact of size and morphology of graphene. *Materials* **2019**, *12*, 842.
[110] Zhou, X. F.; Wang, F.; Zhu, Y. M.; Liu, Z. P. Graphene modified $LiFePO_4$ cathode materials for high power lithium ion batteries. *J. Mater. Chem.* **2011**, *21*, 3353–3358.
[111] Wei, W.; Lv, W.; Wu, M. B.; Su, F. Y.; He, Y. B.; Li, B. H.; Kang, F. Y.; Yang, Q. H. The effect of graphene wrapping on the performance of $LiFePO_4$ for a lithium ion battery. *Carbon* **2013**, *57*, 530–533.
[112] Tian, X. H.; Zhou, Y. K.; Tu, X. F.; Zhang, Z. T.; Du, G. D. Well-dispersed $LiFePO_4$ nanoparticles anchored on a three-dimensional graphene aerogel as high-performance positive electrode materials for lithium-ion batteries. *J. Power Sources* **2017**, *340*, 40–50.
[113] Wang, H. B.; Maiyalagan, T.; Wang, X. Review on recent progress in nitrogen-doped graphene: Synthesis, characterization, and its potential applications. *ACS Catal.* **2012**, *2*, 781–794.
[114] Wang, B.; Al Abdulla, W.; Wang, D. L.; Zhao, X. S. A three-dimensional porous $LiFePO_4$ cathode material modified with a nitrogen-doped graphene aerogel for high-power lithium ion batteries. *Energy Environ. Sci.* **2015**, *8*, 869–875.
[115] Wang, H. L.; Yang, Y.; Liang, Y. Y.; Cui, L. F.; Casalongue, H. S.; Li, Y. G.; Hong, G. S.; Cui, Y.; Dai, H. J. $LiMn_{1-x}Fe_xPO_4$ nanorods grown on graphene sheets for ultrahigh-rate-performance lithium ion batteries. *Angew. Chem., Int. Ed.* **2011**, *50*, 7364–7368.
[116] Rui, X. H.; Sim, D. H.; Wong, K. M.; Zhu, J. X.; Liu, W. L.; Xu, C.; Tan, H. T.; Xiao, N.; Hng, H. H.; Lim, T. M. et al. $Li_3V_2(PO_4)_3$ nanocrystals embedded in a nanoporous carbon matrix supported on reduced graphene oxide sheets: Binder-free and high rate cathode material for lithium-ion batteries. *J. Power Sources* **2012**, *214*, 171–177.
[117] Bak, S. M.; Nam, K. W.; Lee, C. W.; Kim, K. H.; Jung, H. C.; Yang, X. Q.; Kim, K. B. Spinel $LiMn_2O_4$/reduced graphene oxide hybrid for high rate lithium ion batteries. *J. Mater. Chem.* **2011**, *21*, 17309–17315.
[118] Chen, Z. H.; Belharouak, I.; Sun, Y. K.; Amine, K. Titanium-based anode materials for safe lithium-ion batteries. *Adv. Funct. Mater.* **2013**, *23*, 959–969.
[119] Tsai, P. C.; Hsu, W. D.; Lin, S. K. Atomistic structure and *ab initio* electrochemical properties of $Li_4Ti_5O_{12}$ defect spinel for Li ion batteries. *J. Electrochem. Soc.* **2014**, *161*, A439–A444.
[120] Mhamane, D.; Aravindan, V.; Taneja, D.; Suryawanshi, A.; Game, O.; Srinivasan, M.; Ogale, S. Graphene based nanocomposites for alloy (SnO_2), and conversion (Fe_3O_4) type efficient anodes for Li-ion battery applications. *Compos. Sci. Technol.* **2016**, *130*, 88–95.
[121] He, H. Y.; Fu, W.; Wang, H. T.; Wang, H.; Jin, C. H.; Fan, H. J.; Liu, Z. Silica-modified SnO_2-graphene "slime" for self-enhanced Li-ion battery anode. *Nano Energy* **2017**, *34*, 449–455.
[122] Dou, Y. H.; Xu, J. T.; Ruan, B. Y.; Liu, Q. N.; Pan, Y. D.; Sun, Z. Q.; Dou, S. X. Atomic layer-by-layer Co_3O_4/graphene composite for high performance lithium-ion batteries. *Adv. Energy Mater.* **2016**, *6*, 1501835.
[123] Wu, Z. S.; Ren, W. C.; Wen, L.; Gao, L. B.; Zhao, J. P.; Chen, Z. P.; Zhou, G. M.; Li, F.; Cheng, H. M. Graphene anchored with Co_3O_4 nanoparticles as anode of lithium ion batteries with enhanced reversible capacity and cyclic performance. *ACS Nano* **2010**, *4*, 3187–3194.
[124] Jiang, Y.; Yan, X. M.; Xiao, W.; Tian, M. L.; Gao, L.; Qu, D. Y.; Tang, H. L. Co_3O_4-graphene nanoflowers as anode for advanced lithium ion batteries with enhanced rate capability. *J. Alloys Compd.* **2017**, *710*, 114–120.
[125] Huang, M. B.; Chen, C. H.; Wu, S. P.; Tian, X. D. Remarkable high-temperature Li-storage performance of few-layer graphene-anchored Fe_3O_4 nanocomposites as an anode. *J. Mater. Chem. A* **2017**, *5*, 23035–23042.
[126] Li, L.; Wang, H. L.; Xie, Z. J.; An, C. H.; Jiang, G. X.; Wang, Y. J. 3D graphene-encapsulated nearly monodisperse Fe_3O_4 nanoparticles as high-performance lithium-ion battery anodes. *J. Alloys Compd.* **2020**, *815*, 152337.
[127] Xiang, Y.; Zhang, W. F.; Chen, B.; Jin, Z. Q.; Zhang, H.; Zhao, P. C.; Cao, G. P.; Meng, Q. Q. Nano-$Li_4Ti_5O_{12}$ particles *in-situ* deposited on compact holey-graphene framework for high volumetric power capability of lithium ion battery anode. *J. Power Sources* **2020**, *447*, 227372.
[128] Li, C.; Zhao, M.; Sun, C. N.; Jin, B.; Yang, C. C.; Jiang, Q. Surface-amorphized TiO_2 nanoparticles anchored on graphene as anode materials for lithium-ion batteries. *J. Power Sources* **2018**, *397*, 162–169.
[129] Li, L.; Raji, A. R. O.; Tour, J. M. Graphene-wrapped MnO_2-graphene nanoribbons as anode materials for high-performance lithium ion batteries. *Adv. Mater.* **2013**, *25*, 6298–6302.
[130] Yang, M.; Liu, J. X.; Li, S. K.; Zhang, S.; Wang, Y. C.; He, C. Ultrafast synthesis of graphene nanosheets encapsulated Si nanoparticles via deflagration of energetic materials for lithium-ion batteries. *Nano Energy* **2019**, *65*, 104028.
[131] Xue, H. L.; Wang, J.; Wang, S. S.; Muhammad, S.; Feng, C. H.; Wu, Q.; Li, H. S.; Shi, D. X.; Jiao, Q. Z.; Zhao, Y. Core-shell MoS_2@graphene composite microspheres as stable anodes for Li-ion batteries. *New J. Chem.* **2018**, *42*, 15340–15345.
[132] Hagen, M.; Hanselmann, D.; Ahlbrecht, K.; Maça, R.; Gerber, D.; Tubke, J. Lithium-sulfur cells: The gap between the state-of-the-art and the requirements for high energy battery cells. *Adv. Energy Mater.* **2015**, *5*, 1401986.
[133] Wang, M. Z.; Yang, H.; Wang, K. X.; Chen, S. L.; Ci, H. N.; Shi, L. R.; Shan, J. Y.; Xu, S. P.; Wu, Q. C.; Wang, C. Z. et al. Quantitative analyses of the interfacial properties of current collectors at the mesoscopic level in lithium ion batteries by using hierarchical graphene. *Nano Lett.* **2020**, *20*, 2175–2182.
[134] Mo, R. W.; Rooney, D.; Sun, K. N.; Yang, H. Y. 3D nitrogen-doped graphene foam with encapsulated germanium/nitrogen-doped graphene yolk-shell nanoarchitecture for high-performance flexible Li-ion battery. *Nat. Commun.* **2017**, *8*, 13949.
[135] Shin, D. Y.; Ahn, H. J. Interfacial engineering of a heteroatom-doped graphene layer on patterned aluminum foil for ultrafast lithium storage kinetics. *ACS Appl. Mater. Interfaces* **2020**, *12*, 19210–19217.
[136] Shen, W.; Li, K.; Lv, Y. Y.; Xu, T.; Wei, D.; Liu, Z. F. Highly-safe and ultra-stable all-flexible gel polymer lithium ion batteries aiming for scalable applications. *Adv. Energy Mater.* **2020**, *10*, 1904281.

[137] Xu, H. L.; Jin, H. C.; Qi, Z. K.; Guo, Y.; Wang, J. X.; Zhu, Y. W.; Ji, H. X. Graphene foil as a current collector for NCM material-based cathodes. *Nanotechnology* **2020**, *31*, 205710.

[138] Chen, Y. N.; Fu, K.; Zhu, S. Z.; Luo, W.; Wang, Y. B.; Li, Y. J.; Hitz, E.; Yao, Y. G.; Dai, J. Q.; Wan, J. Y. et al. Reduced graphene oxide films with ultrahigh conductivity as Li-ion battery current collectors. *Nano Lett*. **2016**, *16*, 3616–3623.

[139] Rana, K.; Singh, J.; Lee, J. T.; Park, J. H.; Ahn, J. H. Highly conductive freestanding graphene films as anode current collectors for flexible lithium-ion batteries. *ACS Appl*. *Mater*. *Interfaces* **2014**, *6*, 11158–11166.

[140] Jiang, J. M.; Nie, P.; Ding, B.; Wu, W. X.; Chang, Z.; Wu, Y. T.; Dou, H.; Zhang, X. G. Effect of graphene modified Cu current collector on the performance of $Li_4Ti_5O_{12}$ anode for lithium-ion batteries. *ACS Appl*. *Mater*. *Interfaces* **2016**, *8*, 30926–30932.

[141] Liu, X. F.; Wang, D.; Zhang, B. S.; Luan, C.; Qin, T. T.; Zhang, W.; Wang, D.; Shi, X. Y.; Deng, T.; Zheng, W. T. Vertical graphene nanowalls coating of copper current collector for enhancing rate performance of graphite anode of Li ion battery: The merit of optimized interface architecture. *Electrochim*. *Acta* **2018**, *268*, 234–240.

[142] Wen, L.; Liang, J.; Liu, C. M.; Chen, J.; Huang, Q. G.; Luo, H. Z.; Li, F. $Li_4Ti_5O_{12}$ on graphene for high rate lithium ion batteries. *J*. *Electrochem*. *Soc*. **2016**, *163*, A2951–A2955.

[143] Su, F. Y.; Tang, R.; He, Y. B.; Zhao, Y.; Kang, F. Y.; Yang, Q. H. Graphene conductive additives for lithium ion batteries: Origin, progress and prospect. *Chin*. *Sci*. *Bull*. **2017**, *62*, 3743–3756.

[144] Wei, X. F.; Guan, Y. B.; Zheng, X. H.; Zhu, Q. Z.; Shen, J. R.; Qiao, N.; Zhou, S. Q.; Xu, B. Improvement on high rate performance of $LiFePO_4$ cathodes using graphene as a conductive agent. *Appl*. *Surf*. *Sci*. **2018**, *440*, 748–754.

[145] Liu, T. F.; Zhao, L.; Zhu, J. S.; Wang, B.; Guo, C. F.; Wang, D. L. The composite electrode of $LiFePO_4$ cathode materials modified with exfoliated graphene from expanded graphite for high power Li-ion batteries. *J*. *Mater*. *Chem*. A **2014**, *2*, 2822–2829.

[146] Li, X. L.; Zhang, Y. L.; Song, H. F.; Du, K.; Wang, H.; Li, H. Y.; Huang, J. M. The comparison of carbon conductive additives with different dimensions on the electrochemical performance of $LiFePO_4$ cathode. *Int*. *J*. *Electrochem*. *Sci*. **2012**, *7*, 7111–7120.

[147] Rai, A. K.; Gim, J.; Kang, S. W.; Mathew, V.; Anh, L. T.; Kang, J.; Song, J.; Paul, B. J.; Kim, J. Improved electrochemical performance of $Li4Ti_5O_{12}$ with a variable amount of graphene as a conductive agent for rechargeable lithium-ion batteries by solvothermal method. *Mater*. *Chem*. *Phys*. **2012**, *136*, 1044–1051.

[148] Zhang, B.; Yu, Y.; Liu, Y. S.; Huang, Z. D.; He, Y. B.; Kim, J. K. Percolation threshold of graphenenanosheets as conductive additives in $Li_4Ti_5O_{12}$ anodes of Li-ion batteries. *Nanoscale* **2013**, *5*, 2100–2106.

[149] Sun, D. P.; Tian, X. Z.; Ke, F.; Zhang, J. Competition and synergy of carbon nanomaterials in lithium-ion battery. *Sci*. *Sin*. *Chim*. **2020**, *50*, 1333–1343.

[150] Chen, H. W.; Zhang, H. X.; Wu, Y. H.; Zhang, T.; Guo, Y. C.; Zhang, Q. H.; Zeng, Y. J.; Lu, J. G. Nanostructured Nb_2O_5 cathode for high-performance lithium-ion battery with Super-P and graphene compound conductive agents. *J*. *Electroanal*. *Chem*. **2018**, *827*, 112–119.

[151] Jiang, R. Y.; Cui, C. Y.; Ma, H. Y. Using graphenenanosheets as a conductive additive to enhance the rate performance of spinel $LiMn_2O_4$ cathode material. *Phys*. *Chem*. *Chem*. *Phys*. **2013**, *15*, 6406–6415.

[152] Wen, F.; Yang, B.; Huang, G. J.; Zhang, S. H. Progress in application research of graphene-based conductive additive in lithium ion batteries. *Electron*. *Compon*. *Mater*. **2019**, *38*, 6–13.

[153] Gao, P.; Zhang, Y. L.; Yan, J. Effects of graphene/carbon nanotube composite conductive agent to $LiNi_{1/3}Co_{1/3}Mn_{1/3}O_2$. *Battery Bimon*. **2017**, *47*, 339–342.

[154] He, X. Z.; Hu, Y.; Deng, Z. D.; Kong, L. Y.; Shang, W. L. Effect of graphene composite conductive agent SP/CNTs/G on performance of $LiNi_{0.5}Co_{0.2}Mn_{0.3}O_2$ lithium-ion battery. *Electron*. *Compon*. *Mater*. **2016**, *35*, 77–82.